



An 8-aminoquinoline-naphthyl copper complex causes apoptotic cell death by modulating the expression of apoptotic regulatory proteins in breast cancer cells

Nonzuzo Myeza^a, Cathy Slabber^b, Orde Q. Munro^{b,c}, Sheldon Sookai^b, Savannah C. Zacharias^d, Carla Martins-Furness^a, Leonie Harmse^{a,*}

^a Division of Pharmacology, Department of Pharmacy and Pharmacology, Faculty of Health Sciences, University of the Witwatersrand, 7 York Road, Parktown, 2193, South Africa

^b Molecular Sciences Institute, School of Chemistry, University of the Witwatersrand, 1 Jan Smut Ave, Braamfontein, Johannesburg, 2017, South Africa

^c School of Chemistry, University of Leeds, Woodhouse Lane, Leeds, LS2 9JT, UK

^d School of Chemistry and Physics, University of KwaZulu-Natal, King Edward Drive, Pietermaritzburg, Scottsville, 3209, South Africa

ARTICLE INFO

Keywords:

8-Aminoquinoline-naphthyl-copper complex

Apoptosis

Inhibitor of apoptosis proteins

Haem oxygenase-1

Breast cancer

ABSTRACT

Breast cancer is one of the most common cancers globally and a leading cause of cancer-related deaths among women. Despite the combination of chemotherapy with targeted therapy, including monoclonal antibodies and kinase inhibitors, drug resistance and treatment failure remain a common occurrence. Copper, complexed to various organic ligands, has gained attention as potential chemotherapeutic agents due to its perceived decreased toxicity to normal cells. The cytotoxic efficacy and the mechanism of cell death of an 8-aminoquinoline-naphthyl copper complex (Cu8AqN) in MCF-7 and MDA-MB-231 breast cancer cell lines was investigated. The complex inhibited the growth of MCF-7 and MDA-MB-231 cells with IC₅₀ values of 2.54 ± 0.69 μM and 3.31 ± 0.06 μM, respectively. Nuclear fragmentation, annexin V binding, and increased caspase-3/7 activity indicated apoptotic cell death. The loss of mitochondrial membrane potential, an increase in caspase-9 activity, the absence of active caspase-8 and a decrease of tumour necrosis factor receptor 1 (TNFR1) expression supported activation of the intrinsic apoptotic pathway. Increased ROS formation and increased expression of haem oxygenase-1 (HMOX-1) indicated activation of cellular stress pathways. Expression of p21 protein in the nuclei was increased indicating cell cycle arrest, whilst the expression of inhibitor of apoptosis proteins (IAPs); cIAP1, XIAP and survivin were decreased, creating a pro-apoptotic environment. Phosphorylated p53 species; phospho-p53(S15), phospho-p53(S46), and phospho-p53(S392) accumulated in MCF-7 cells indicating the potential of Cu8AqN to restore p53 function in the cells. In combination, the data indicates that Cu8AqN is a useful lead molecule worthy of further exploration as a potential anti-cancer drug.

1. Introduction

Breast cancer is a leading cause of cancer-related deaths among women (Sung et al., 2021). Treatment regimens are designed following staging and molecular profiling to achieve the best possible outcomes (Sarhangi et al., 2022). The absence of receptors for oestrogen, progesterone, and the human epidermal growth factor-2 receptor is associated with a poor prognosis (Joshi and Press, 2018). The standard of care includes surgical resection, radiotherapy, chemotherapy and targeted therapy (Waks and Winer, 2019). Chemotherapy includes cyclophosphamide, doxorubicin, paclitaxel in combination with targeted

treatments like trastuzumab and immune checkpoint inhibitors like pembrolizumab (Harbeck, 2022; Emens and Loi, 2023). Despite the advances made, drug resistance and treatment failure is common in triple-negative breast cancer and metastatic disease. Both targeted and traditional chemotherapeutic agents are associated with severe adverse drug reactions, contributing to patient morbidity and driving the notion to de-escalate treatments (Sacchini and Norton, 2022). Consequently, the search for alternative treatments remains important.

Copper complexed to various organic ligands have potential as chemotherapeutic agents due to their predicted lower toxicity to normal cells, compared with platinum containing chemotherapeutic drugs

* Corresponding author.

E-mail address: Leonie.Harmse@wits.ac.za (L. Harmse).

<https://doi.org/10.1016/j.ejphar.2024.176764>

Received 27 February 2024; Received in revised form 8 June 2024; Accepted 19 June 2024

Available online 20 June 2024

0014-2999/© 2024 The Authors. Published by Elsevier B.V. This is an open access article under the CC BY-NC license (<http://creativecommons.org/licenses/by-nc/4.0/>).

(McGivern et al., 2018; Zehra et al., 2021a, 2021b; Balsa et al., 2023). Since copper functions as a co-factor in specific enzymatic reactions in humans, its transport and distribution are finely controlled (Matson-Dzebo et al., 2016; Yang et al., 2023). Hitherto, successful development of Cu(II) metallodrugs is exemplified by both Elesclomol and Casiopeina III-ia (Tarin et al., 2023; Aguilar-Jiménez et al., 2022).

Investigational polypyridine copper complexes reportedly bind and inhibit the 20S proteasome causing apoptosis in triple negative breast cancer cell lines, MDA-MB-231 and CAL-5 Li et al. (2019). Foo et al. (2018), reported IC₅₀ values ~20 µM with apoptotic cell death for S-benzylidithiocarbamate copper complexes in MDA-MB-231 cells. Gordon et al. (2022) reported IC₅₀ values of 1.5 µM and 2.6 µM for MDA-MB-231 and MCF-7 cells for a copper-phenanthroline-theophylline complex. Copper complexes of imidazo[1,2-*a*]pyridines were active against five cell lines including breast cancer cell lines (Dam et al., 2017). These complexes induced intrinsic apoptosis in HT-29 colorectal and leukaemic cell lines by modulating the transcriptional activity of the NF-κB pathway (Harmse et al., 2019; Ismail et al., 2022).

The ligand critically controls the efficacy and selectivity of copper complexes (Ali et al., 2021). The 8-aminoquinoline ligand is known for its metal chelating ability and rigid structure., (Facchetti et al., 2019; Ali et al., 2021). A Pt(II)-8-aminoquinoline derivative induced p53 and suppressed the growth of MDA-MB-231 triple-negative breast cancer cells, with the most active complex having an IC₅₀ value of 10.9 ± 1.3 µM (Facchetti et al., 2019).

This study reports the superior cytotoxic efficacy, mechanism of cell death and effects on apoptotic regulatory proteins of an 8-aminoquinoline-naphthyl copper complex (Cu8AqN) in MDA-MB-231 and MCF-7 breast cancer cell lines. We investigated its effect on two important cancer related proteins, HMOX-1 and the tumour suppressor protein, p21. To our knowledge, this is the first study to report on the cytostatic effect and cell death mechanisms of Cu8AqN in breast cancer cell lines.

2. Methods

2.1. Synthesis, characterization and stability of 8AqN and Cu8AqN

General methods, instruments, and materials used for compound synthesis and biochemistry are given in the Supplementary data. Information relevant to the cell biology experiments is contained in the main body of the manuscript.

2.1.1. Compound synthesis and characterization and purity

Complete details for the synthesis and characterization of the compounds reported herein, specifically the metal-free ligand 1-[(*E*)-8-quinolyliminomethyl]naphthalen-2-ol, abbreviated 8AqN, and the Cu(II) chelate of this ligand, Cu8AqN, are given in the Supplementary data. The protocol followed was described previously by Zacharias (2012) and later by Kozlyuk et al., 2015.

Purity of 8AqN: The compound was synthesized in ethanol, affording a bright orange product as a fine precipitate. Recrystallization from acetonitrile afforded orange needle-like crystals. The crystalline material had a purity of 99% (1% ethanol) based on its NMR peak integration data (Fig. S2). From the microanalytical elemental analysis data for the bulk powder material (C, H, and N), the mean percentage purity of the bulk solid compound was ~97%. Because the compound was synthesized in ethanol and recrystallized from acetonitrile, residual acetonitrile and ethanol were present (~3%). These trace components were inconsequential for the synthesis of the metal chelate and any *in vitro* cell biology work.

Purity of Cu8AqN: As described in Supplementary data, the metal chelate was synthesized by reacting the ligand with CuCl₂·2H₂O in hot ethanol and then recrystallized as an orange-brown solid from ethanol. From the microanalytical elemental analysis data (C, H, and N), the mean percentage purity of the bulk solid compound was 97.3%. The residual component (2.7%) was ethanol.

2.1.2. Plasma stability assays

The UV-visible spectra of 63 µM Cu8AqN, AqN, 8-aminoquinoline and 2-hydroxy-4-naphthaldehyde were analysed in human plasma (National Bioproduct Institute, South Africa) as a function of time over 24 h or 36 h at 37 °C (unless otherwise stated). Plasma was diluted in phosphate buffer (50 mM; pH 7.50) in a 1:4 ratio. Spectra for control compounds and Cu8AqN were also measured in water/DMSO or phosphate buffer (50 mM, pH 7.50). Each spectrum was recorded from 200 to 800 nm using a Specord-210 Plus double beam spectrometer (Analytik-Jena, Germany). The temperature was regulated using thermostatic cell holders connected to a circulating water bath with a temperature accuracy of ±0.5 °C. Three independent experiments were performed for Cu8AqN. Data points for determination of the half-life of Cu8AqN were averaged for plotting and curve fitting.

2.2. Cell culture

The breast cancer cell lines MCF-7 and MDA-MB-231 and the normal breast cell line MCF-10A were obtained from the ATCC (Manassas, Virginia). MDA-MB-231 and MCF-7 breast cancer cell lines both represent invasive breast adenocarcinomas but differ in their molecular characteristics. MCF-7 cells are oestrogen and progesterone dependent and is a good model for oestrogen receptor positive breast cancer. MDA-MB-231 cells lack the expression of the receptors for oestrogen, progesterone and human epidermal growth factor-2 and represents triple-negative breast cancer (Theodossiou et al., 2019). Cell lines were evaluated for authenticity by Inqaba Biotech, SA, using Short Tandem Repeat (STR) profiling. All cell lines were regularly evaluated for mycoplasma infection by fluorescence microscopy with the Hoechst 33342 DNA stain.

The cells were maintained in a humidified incubator at 37°C in a 5% CO₂ atmosphere. MCF-7 and MDA-MB-231 breast cancer cells were cultured in 1:1 ratio of DMEM/Ham's F12 media (Gibco, ThermoFisher, South Africa), supplemented with 10% heat inactivated foetal bovine serum (Gibco, ThermoFisher, South Africa). MCF-10A cells were cultured in modified basal serum-free media for mammary epithelium cells containing human epidermal growth factor (20 ng/ml), insulin (0.01 mg/ml), hydrocortisone (500 ng/ml), bovine pituitary extract (25 mg), and isoproterenol transferrin (Gibco, ThermoFisher, South Africa).

2.3. Selection of compounds and treatment concentrations

The 8-aminoquinoline-naphthyl copper (II) complex (Cu8AqN) and the 8-aminoquinoline-naphthyl copper free ligand (8AqN) were synthesized and fully characterized as described in Section 2.1.1. Doxorubicin, (Sigma Aldrich, South Africa), was selected as a positive control since it is used clinically in the treatment of metastatic breast cancer whereas the platinum drugs are rarely used. Doxorubicin is an anthracycline and causes apoptosis by intercalating with the DNA. It directly inhibits DNA replication and repair by inhibiting the re-ligation function of the topoisomerase II enzyme causing DNA double strand breaks (Wang et al., 2004). Cisplatin on the other hand is unstable in aqueous environments and act by forming covalent adducts with DNA (Takahara et al., 1995). Untreated cells were used as negative controls. Cu8AqN, 8AqN and doxorubicin was dissolved in cell culture grade dimethyl sulfoxide (DMSO) (PanReac AppliChem, South Africa) at concentrations of 3 mM and 10 mM for Cu8AqN and 8AqN respectively, while doxorubicin was prepared at a concentration of 10 mM. The cells were treated with freshly diluted compounds.

2.4. Cytotoxicity studies

The MTT (3-(4,5-dimethylthiazol-2-yl)-2,5-diphenyl tetrazolium bromide) assay was used to evaluate the effect of the complexes on the cells and determine the IC₅₀ values. The assay was performed as described in the literature by Mosmann (1983), and modified by

dissolving the formazan crystals in dimethyl sulfoxide (Sigma Aldrich, South Africa). Cells were seeded at 10 000 cells per well in 100 μ l of culture media in 96-well plates (Nest, Whitehead Scientific, SA) and allowed to adhere overnight. The next day, the cells were treated with 100 μ l of media containing a range of concentrations of Cu8AqN, 8AqN and doxorubicin. Each concentration was tested in quadruplicate and experiments were repeated at least three times. After a 44 hours (h) incubation at 37 °C, 40 μ l of MTT solution (5 mg/ml) was added to each well, followed by a further 4 h incubation. The plates were centrifuged at 735 \times g for 5 min (min) to ensure sedimentation of the formazan crystals. Thereafter, culture media and the MTT solution was removed. The formazan crystals were dissolved in 200 μ l DMSO and the absorbance of the solubilized formazan crystals was measured at 540 nm and 690 nm with a Labsystems iEMS plate reader (ThermoLabsystems, Finland). The percentage cell viability was calculated and the IC₅₀ values were determined from a sigmoidal log dose-response curve generated by GraphPad Prism software Version 10.

2.5. Evaluation of cellular morphology and necrosis

Fluorescent microscopy was used to investigate morphological changes caused by the Cu8AqN, 8AqN and doxorubicin in MCF-7 and MDA-MB-231 breast cancer cells. The fluorochromes, propidium iodide (ThermoFisher, South Africa), and Hoechst33342 (Sigma Aldrich, South Africa) were used to assess nuclear changes. The assay was performed as previously described by (Harmse et al., 2015). MCF-7 and MDA-MB-231 cells were seeded on sterile glass coverslips in 6-well culture plates and incubated with 2 mL culture media overnight in a humidified incubator at 37 °C with 5% CO₂ atmosphere. The following day, the cells were treated with Cu8AqN, 8AqN and doxorubicin at a final concentration equivalent to the IC₈₀ value of each complex for 18 h. Following washing with PBS, the coverslips were incubated with a Hoechst/Propidium iodide mixture (Hoechst-33342 concentration was 5 μ g/mL, and propidium iodide was 10 μ g/mL) for 20 min in the dark at room temperature. The coverslips were rinsed with PBS, mounted on microscope slides, and viewed with an Olympus BX41 microscope, using the U-MWIG2 and U-MWU2 Olympus filter cubes for propidium iodide and Hoechst 33342, respectively. Images were captured with an Olympus DP72 camera and analysed with the Olympus CellSens Software (Olympus, Tokyo, Japan).

2.6. Annexin V assay

The Annexin-V-FLOUS staining kit (Roche, Mannheim, Germany) was used to investigate the presence of phosphatidylserine on the outer leaflet of the cell membrane of the treated and untreated MCF-7 and MDA-MB-231 cells. Cells were grown on coverslips and treated as described in Section 2.5. At the end of the treatment period, the culture media was removed, and the coverslips were gently rinsed with PBS. The coverslips were mounted on microscope slides with 40 μ l of the Annexin-V-FLOUS and PI working solution and incubated in the dark for 15 min. Thereafter, the slides were viewed, images captured with the Olympus DP72 camera using the U-MNIB3 filter cube for annexin V and U-MWIG2 for propidium iodide. Images were analysed with the Olympus CellSens Software.

2.7. Assessment of reactive oxygen species (ROS) formation

ROS production was measured by CellROX Deep Red Reagent fluorescent probe (Molecular Probes, Life Technologies, South Africa). Cells were treated as above and doxorubicin and tert-butyl-hydro-peroxidase (tBHP) were used as positive controls. The CellROX Deep Red Reagent (2.5 μ M) was added at the same time as the test compounds and incubated for 6 h. At the end of the treatment period, the treatment media was removed, and the coverslips were rinsed with PBS twice and mounted on microscope slides for viewing with an Olympus BX41 microscope, using the U-MWIG2 filter cube to detect the CellROX Deep Red

reagent (excitation/emission of 640/665 nm). Fluorescence intensity was measured with ImageJ software.

2.8. Detection of caspase-3/-7 activity

Caspase-3/7 activity was assessed with the CellEvent™ Caspase-3/7 green detection reagent (Invitrogen, ThermoFisher, South Africa). The assay was performed as instructed by the manufacturer. Cells were plated and treated as described in Section 2.5 for 48 h. At the end of treatment period, the media was removed, and floating cells harvested by centrifugation at 735 g, and the coverslips washed with PBS. Thereafter, the coverslips and the harvested cells were incubated at 37 °C for 30 min with 5 μ M of CellEvent™ Caspase-3/7 detection reagent which selectively binds to active caspase-3. The fluorescent signal was detected with an Olympus BX41 microscope, using the U-MNIB3 filter cube for Caspase-3/7 activity. Images were captured with an Olympus DP72 camera and analysed with the Olympus CellSens Software.

2.9. Assessment of mitochondrial membrane potential ($\Delta\Psi_m$)

The change in mitochondrial membrane potential (MMP) was assessed using the reagent 5',6,6'-tetrachloro-1,1',3,3'-tetraethyl-benzimidazolyl-carbocyanine iodide (JC-1) (ThermoFisher, South Africa). Cells were plated and treated as described in Section 2.5 for 20 h. Post treatment, the cells were rinsed gently with 2 mL of PBS and incubated in the dark for 20 min at 37 °C with 500 μ l of a 5 μ g/mL JC-1 reagent. After removing the reagent, the coverslips were washed and viewed on an Olympus BX41 epifluorescence microscope at 400X magnification using the Olympus U-MWIG2 filter cube for JC-1 aggregates and U-MNIB3 filter cube for JC-1 monomers. Images were captured with an Olympus DP72 camera and analysed using the Olympus CellSens Software package.

2.10. Caspase-8 activity assay

The caspase-8 detection kit (ab65618) (Abcam, Biocom Africa) was used to determine caspase-8 activity. The assay was performed as described by the manufacturer. Cells were treated as described above and treated with the test compounds for 20 h. At the end of treatment period, media was discarded, and the cells washed with PBS after which the cells were incubated for 60 min at 37 °C in a 5% CO₂ atmosphere with 3 μ l Red-IETD-FMK peptide in 900 μ l of caspase-8 proprietary buffer. After the incubation period, the cells were rinsed with the same buffer and mounted on microscope slides. The cells were viewed with an Olympus BX41 microscope at 400X magnification, using the U-MWIG2 filter cube. The photographs were captured and analysed as described previously.

2.11. Caspase-9 activity assay

Active caspase-9 was detected with the Abcam Active caspase-9 FITC detection kit (Abcam ab65615) (Abcam, Biocom Africa, South Africa). The assay was performed as indicated by the manufacturer. Cells were treated as described previously for 48 h. At the end of the treatment period, the media was discarded, and the coverslips were rinsed with PBS. Thereafter, each coverslip was incubated for 45 min with 3 μ l FITC-LEHD-FMK in 900 μ l of caspase-9 buffer in a humidified incubator at 37 °C with 5% CO₂. Following the incubation period, the coverslips were gently rinsed with caspase-9 buffer, mounted on a microscope slide, and viewed with an Olympus BX41 microscope at 400X magnification, using the U-MNIB3 filter cube. The images were captured with Olympus DP72 camera and analysed with the Olympus CellSens Software.

2.12. Assessment of apoptotic protein expression levels

2.12.1. Measurement of protein concentration

The total protein concentration in cell lysates were quantified with the Thermo™ Scientific Pierce™ Detergent Compatible Bradford assay reagent (ThermoFisher, South Africa).

2.12.2. Apoptosis protein profiler array

The Proteome Profiler Human Apoptosis Array Kit (Catalog # ARY009, R&D Systems, Minnesota, USA) was used to detect 35 human apoptosis-related proteins simultaneously. The array was performed as recommended by the manufacturer. Briefly, seven million cells were seeded per flask in 20 mL of culture media and grown overnight in 75 cm³ culture flasks. The next day, the media was discarded, and the cells were treated with fresh media containing Cu8AqN, 8AqN and doxorubicin. The cells were harvested after 18 h before any obvious morphological changes were observed by phase contrast microscopy. The cells were lysed with proprietary lysis buffer-17 to which a protease inhibitor cocktail tablet (Roche, Mannheim, Germany) was added and mixed on a rotating platform for 30 min at 4 °C, after which the cell debris was removed by centrifugation at 14000 g for 5 min at 4 °C (ThermoFisher Sorvall LYNX 4000). An aliquot of the clear lysate was used to determine the protein concentration whilst the remainder of the lysate was kept on ice. Following the protein determination, 400 µg of protein from each treatment was incubated with each of the pre-blocked membranes overnight, at 4 °C, on a rocking platform. On the following day, the membranes were washed 3 times for 10 min with 20 mL of proprietary wash buffer. Thereafter, the membranes were incubated for 1 h with the detection-biotinylated antibody cocktail followed by three wash steps as described above. This was followed by incubation at room temperature for 30 min with horseradish peroxidase conjugated streptavidin. Following this, the membrane arrays were washed as described previously. The membranes were then simultaneously exposed to Chemi-Reagent Mix for 1 min and the chemiluminescent signals captured using the BioRad Chemidoc instrument. The data was analysed using the Biorad Image Lab software Version V (Bio-Rad Laboratories, California, USA).

2.13. Immunofluorescence detection of the cyclin dependent kinase inhibitor, p21 and HMOX-1

The effects of Cu8AqN and doxorubicin on the expression and location of p21 and HMOX-1 (Invitrogen, Life Technologies, South Africa) in MCF-7 and MDA-MB-231 cells were determined with fluorescence microscopy. Cells were seeded on coverslips and treated as described previously. Following treatment, coverslips were rinsed with PBS and fixed for 20 min with 3% formaldehyde in PBS. This was followed by washing and permeabilization for 20 min with 0.25% Triton X100 in PBS containing 0.5% bovine serum albumin (BSA). After permeabilization, the cells were washed as described before and blocked with 0.5% (BSA) in PBS for 1 h. The coverslips were gently washed three times with PBS and incubated at 4°C overnight with a 1:200 dilution of each specific primary antibodies in PBS with 0.5% BSA. On the next day, the coverslips were washed with PBS and incubated with 1:800 dilution of an Alexa fluor 488™ conjugated secondary antibody (ThermoFisher) and Hoechst-33342 for 1 h. Following a washing step, the coverslips were mounted on microscope slides using Fluoromount™ mounting media (Sigma, South Africa) and allowed to dry before viewing with an Olympus BX41 epifluorescence microscope. Images were captured with an Olympus DP72 camera and processed with the Olympus CellSens Software.

2.14. Data analysis

All experiments were performed at least three times and data is presented as a mean and ±standard deviation (SD). The percentage is

expressed as the number of cells with positive fluorescence relative to the total number of cells in the accompanying phase contrast image, and three separate fields were counted for each treatment in every experiment. Data and statistical significance were analysed with GraphPad Prism version 10. Statistical significance between the means of the treated group and the untreated control or the positive control group was determined either with Student's t-test or ANOVA followed by Dunnett's post hoc multiple comparison test. In Dunnett's test each experimental group is compared to the control group and the test requires three or more groups for comparison to the control group. The results were considered statistically significant if the *p*-value was ≤0.05.

3. Results

3.1. Cu8AqN is more active against MCF-7 and MDA-MB-231 breast cancer cells than the MCF10A cell line

The Cu8AqN complex inhibited proliferation of MCF-7 and MDA-MB-231 breast cancer cells with the IC₅₀ values of 2.54 ± 0.99 and 3.31 ± 0.12 µM, respectively (Table 1). It was three-fold less active towards the normal mammary epithelial cell line, MCF-10A, with an IC₅₀ value of 9.45 ± 1.03 µM indicating selectivity towards the cancer cell lines. Cu8AqN was more potent in both cancer cell lines than the copper free ligand, 8AqN, which had IC₅₀ values of 16.93 ± 1.13 µM in MCF-7 cells and 97.33 ± 4.28 µM in MDA-MB-231 cells. In MCF-7 cells, doxorubicin had an IC₅₀ value of 1.38 ± 0.48 µM which was lower than that of Cu8AqN, whilst in MDA-MB-231 cells the doxorubicin IC₅₀ was higher with an IC₅₀ of 8.75 ± 1.74 µM. Doxorubicin had an IC₅₀ value of 2.99 ± 0.1 µM against the MCF-10A cell line, indicating its poor selectivity towards non-cancer cells. The structures of the complexes and IC₅₀ values are shown in Table 1.

3.2. Cu8AqN caused nuclear fragmentation in MCF-7 and MDA-MB-231 breast cancer cells

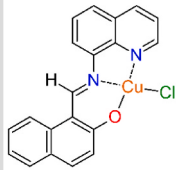
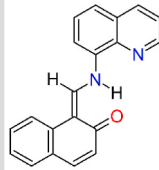
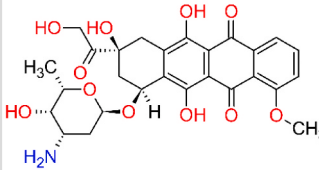
The effects of Cu8AqN and doxorubicin on cell morphology were evaluated in MCF-7 cells, Fig. 1A and MDA-MB-231 cells, Fig. 1B. Untreated MCF-7 breast cancer cells are polygonal, cobblestone-shaped cells with a round to oval evenly stained nucleus as shown in (Fig. 1A, panels a and b). MDA-MB-231 cells shown in (Fig. 1B, panels i and j), are elongated, spindle-like cells with an irregular nucleus. The lack of propidium iodide (PI) staining in (Fig. 1A, panel a–h) and (Fig. 1B, panel i–p), indicate the absence of necrotic cell death. Following treatment with the Cu8AqN complex, both cell types appeared to be smaller and assumed a rounded shape (Fig. 1A, panels c and d), and (Fig. 1B, panels k and l). Hoechst 33342 stained cells treated with Cu8AqN, showed nuclear fragmentation and condensation, (Fig. 1A, panel d) and (Fig. 1B, panel l), which are characteristics consistent with apoptosis. In comparison, the copper free ligand 8AqN caused no obvious changes to the morphology of the cells, (Fig. 1A, panels e and f) and (Fig. 1B, panels m and n). Doxorubicin treated cells were irregular with fragmented nuclei (Fig. 1A, panels g and h), and (Fig. 1B, panels o and p).

3.3. Cu8AqN increased annexin-V binding to phosphatidylserine in breast cancer cells

Annexin-V/propidium iodide binding confirmed early and late (secondary) apoptosis caused by Cu8AqN and doxorubicin as seen in Fig. 2. 8AqN was not included in this assay since it did not cause any significant changes in the cell morphology and had high IC₅₀ values indicating poor efficacy. In the untreated cells of both cell lines (Fig. 2A, panel a and b and Fig. 2C, panel g and h) annexin-V/propidium iodide binding was absent. MCF-7 cells treated with the Cu8AqN complex and doxorubicin (Fig. 2A, panel d and f) and Fig. 2B, predominantly showed annexin-V binding alone as seen by the bright green fluorescence indicative of early apoptosis.

Table 1

The chemical structures of Cu8AqN, the 8AqN copper free ligand and doxorubicin together with their respective IC₅₀ values in MCF-7 and MDA-MB-231 breast cancer cells and the MCF-10A mammary epithelial cell after 48 h of exposure.

	Cu Complex (Cu8AqN)	Copper free Ligand (8AqN)	Doxorubicin
			
Molecular Weight	396.33 g/mol	298.34 g/mol	543.52 g/mol
Cell lines	IC₅₀ values (μM) after 48 h of treatment		
MCF-7	2.54 ± 0.99	16.93 ± 1.13	1.38 ± 0.48
MDA-MB-231	3.31 ± 0.12	97.33 ± 4.28	8.75 ± 1.74
MCF-10A	9.45 ± 1.03	Not determined	2.99 ± 0.1

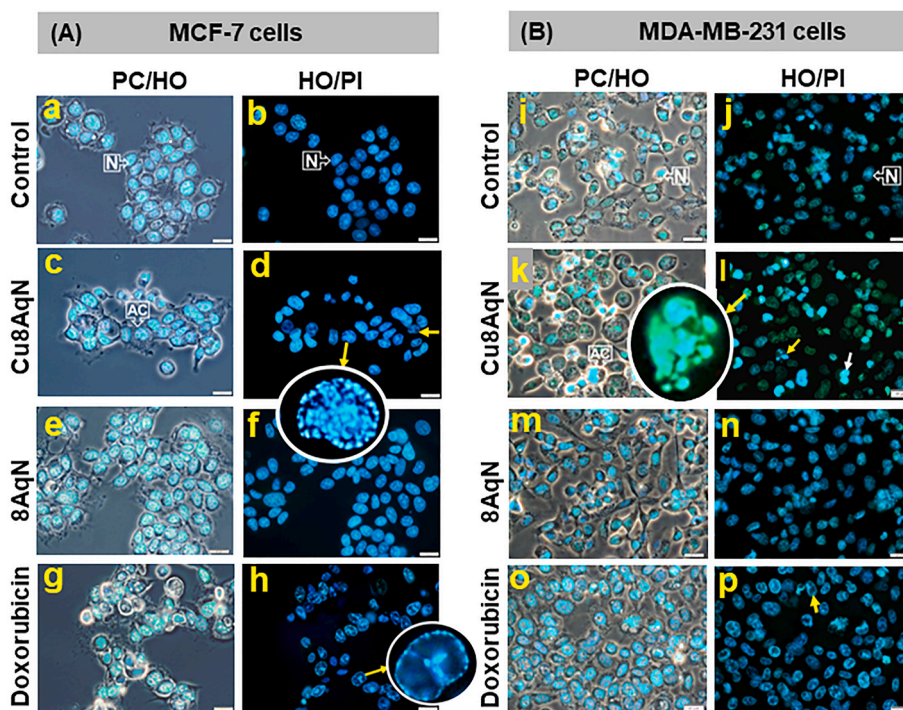


Fig. 1. Cu8AqN caused nuclear fragmentation and condensation in MCF-7 and MDA-MB-231 breast cancer cells. Photomicrographs in part (A) and (B) show the changes to MCF-7 and MDA-MB-231 cells and their nuclei, respectively. The MCF-7 and MDA-MB-231 cells were treated with Cu8AqN at 3 μM and 4.2 μM, respectively. Doxorubicin was used at 5 μM in MCF-7 cells and at 10 μM in MDA-MB-231 cells. The cells were treated for 18 h and viewed with an Olympus BX41 epifluorescence microscope at 400x magnification. Images were captured with an Olympus DP72 camera and analysed with the Olympus CellSens Software. Scalebar: 20 μm. Legend: N = nucleus, white arrow = nuclear condensation, yellow arrow = nuclear fragmentation.

In MDA-MB-231 cells (Fig. 2C, panel j and Fig. 2D), Cu8AqN caused fewer cells to be early apoptotic and more cells to be late apoptotic. In contrast, doxorubicin treated MDA-MB-231 cells showed a high percentage of cells in early apoptosis and a small fraction of cells in late apoptosis. MDA-MB-231 phase contrast images of cells treated with the

Cu8AqN complex, (Fig. 2C, panel i) and doxorubicin, (Fig. 2C, panel k) showed cells with a rounded morphology and fluorescence images which indicated the presence of both early and late apoptotic cells. Cu8AqN caused a higher percentage of cells with late/secondary apoptosis (Fig. 2D) in the cells (22%) compared to doxorubicin, while

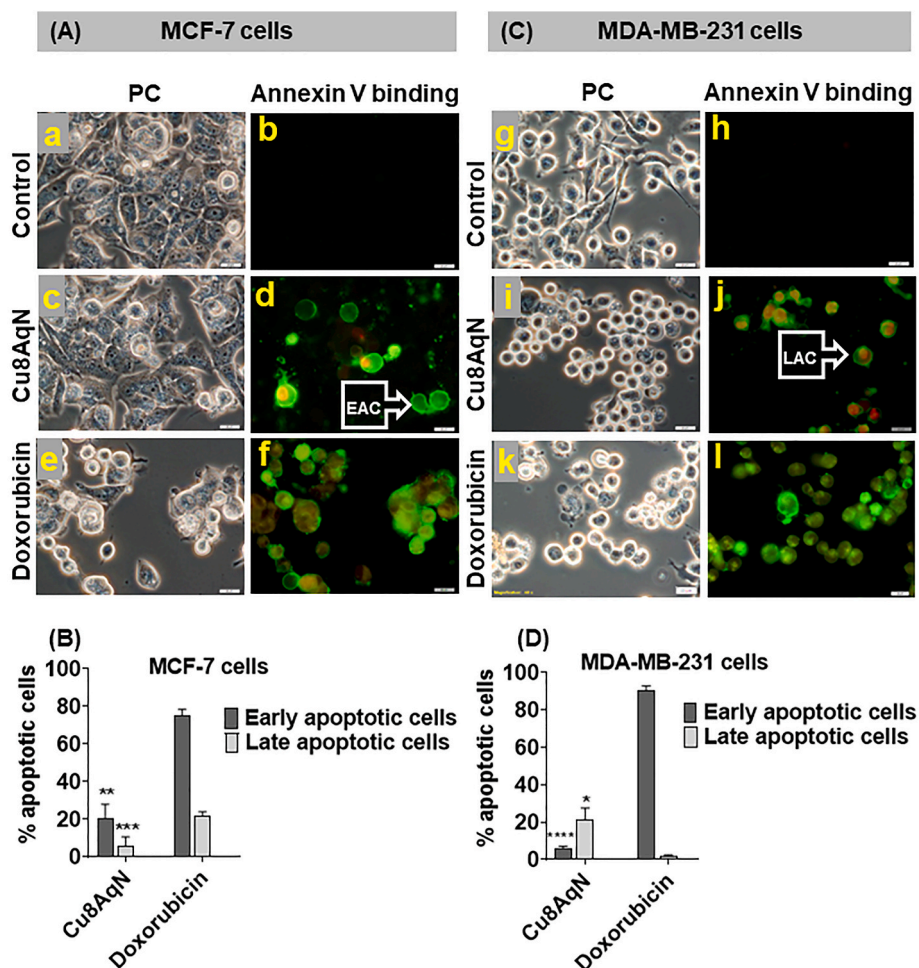


Fig. 2. Photomicrographs showing the increase of Annexin-V binding by Cu8AqN in MCF-7 and MDA-MB-231 cells. (A) is a photomicrograph of Annexin-V binding in MCF-7 cells. (B) is a bar graph showing the percentage of apoptotic cells in MCF-7 cells determined in three separate experiments. (C) shows a photomicrograph of Annexin-V binding in MDA-MB-231 cells. (D) is a bar graph showing the percentage of apoptotic cells from three independent experiments with MDA-MB-231 cells. The MCF-7 and MDA-MB-231 cells were treated with Cu8AqN at 3 μ M and 4.2 μ M, respectively. Doxorubicin was used at 5 μ M in MCF-7 cells and at 10 μ M in MDA-MB-231 cells. The cells were treated for 18 h and viewed with an Olympus BX41 epifluorescence microscope at 400x magnification. Images were captured with an Olympus DP72 camera and analysed with the Olympus CellSens Software. Scalebar: 20 μ m. Legend: EAC = early apoptotic cells, LAC = late apoptotic cells.

doxorubicin showed a higher percentage of cells in early apoptosis (80%). The results of three independent experiments (Fig. 2B and 2D) indicated that doxorubicin was superior to the Cu8AqN complex in causing phosphatidyl serine exposure on the outer cell membrane.

3.4. Cu8AqN increases ROS formation in MCF-7 cells and MDA-MB-231 cells

Since copper complexes are known to cause oxidative stress, the formation of ROS was evaluated (Zehra et al., (b)2021). Low baseline levels of ROS were observed in untreated MCF-7 cells, (Fig. 3A, panels a and b) which was not increased by Cu8AqN (Fig. 3A, panel d and Fig. 3B). Doxorubicin treated cells increased ROS relative to the untreated cells, (Fig. 3A, panel f and Fig. 3B). In MDA-MB-231 cells tBHP was used as a positive control. MDA-MB-231 untreated cells showed low levels of ROS as seen in (Fig. 3C, panels g and h). The Cu8AqN complex and tBHP caused a marked increase of ROS formation in the cells (Fig. 3C, panel j and l and Fig. 3D) with Cu8AqN being a superior inducer when compared with tBHP as reflected in Fig. 3C (panels j and l) and in Fig. 3D.

3.5. Cu8AqN affects mitochondrial function in MCF-7 and MDA-MB-231 cells

3.5.1. Cu8AqN caused a loss of mitochondrial membrane potential ($\Delta\Psi_m$)

In the untreated MCF-7 and MDA-MB-231 cells, (Fig. 4A, panel a) and (Fig. 4C, panel d), J-aggregates were visible as punctate bright red/orange fluorescence and were quantified in Fig. 4B and D, indicating an intact mitochondrial membrane. In the cells treated with Cu8AqN and doxorubicin the monomeric form of JC-1 pre-dominates as seen by the intense green fluorescence and absence of red fluorescence (Fig. 4A, panel b and c; Fig. 4B) and (Fig. 4C, panel e and f; Fig. 4D), indicating a loss of mitochondrial membrane potential. The diffuse green fluorescence caused by Cu8AqN and doxorubicin in both cell lines indicates that the mitochondria are no longer intact. Depolarized but intact mitochondria have a punctate appearance with green fluorescence.

3.5.2. Cu8AqN increased caspase-9 activity in MCF-7 and MDA-MB-231 cells

Caspase-9 activity was not present in the untreated controls of MCF-7 (Fig. 5A, panel a and b) and MDA-MB-231 cells (Fig. 5B, panel g and h) cells. The treatment of MCF-7, (Fig. 5A, panel c, d, e, and f) and MDA-MB-231 (Fig. 5B, panels i, j, k and l) cells with Cu8AqN and doxorubicin caused the activation of caspase-9 in close to 100% of the cells. In

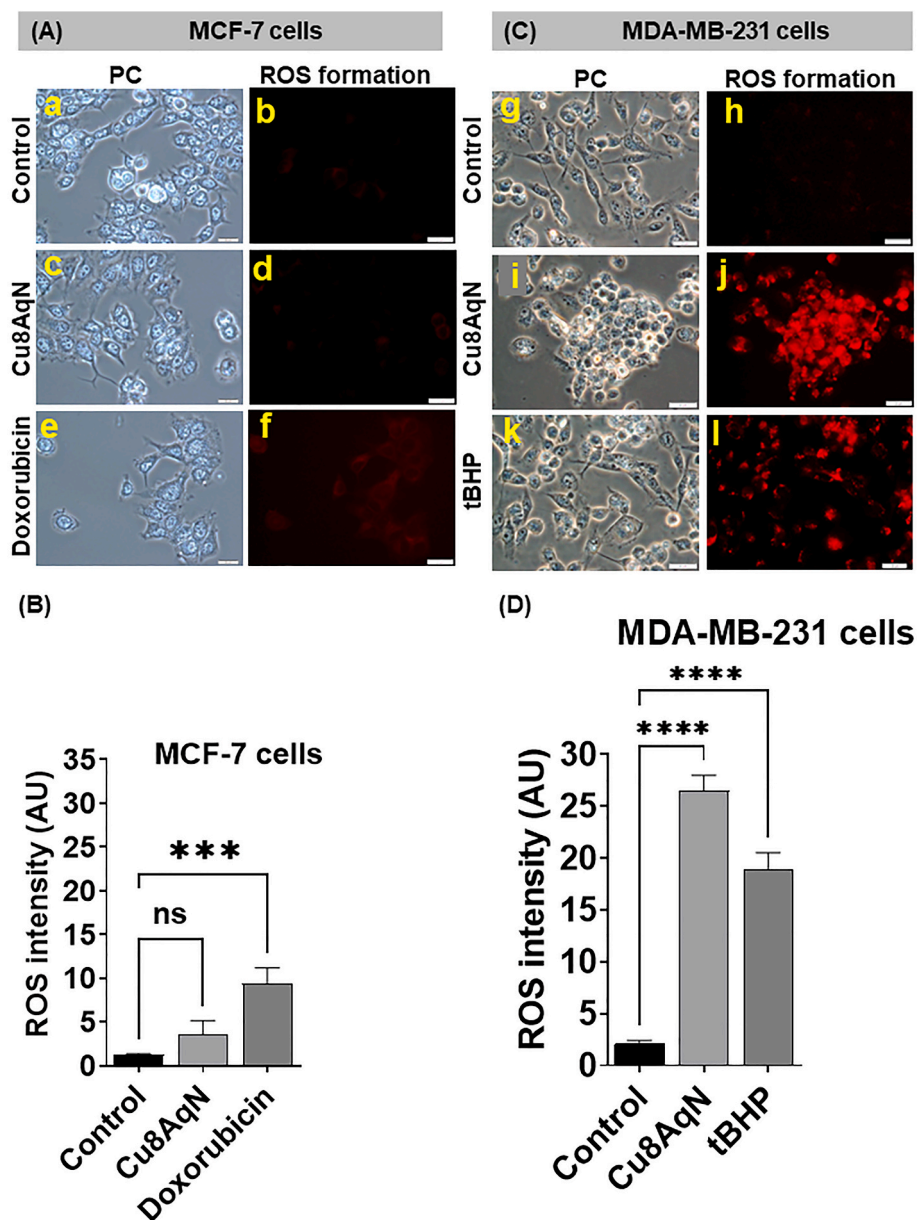


Fig. 3. Cu8AqN increased the formation of reactive oxygen species (ROS) in MCF-7 and MDA-MB-231 breast cancer cells. (A) is a representative photomicrograph of a ROS formation in MCF-7 cells, (B) is a bar graph of three independent experiments determining ROS intensity in MCF-7 cells. (C) is a representative photomicrograph of ROS formation in MDA-MB-231 cells. (D) is a bar graph of three independent experiments determining ROS intensity in MDA-MB-231 cells. MCF-7 cells were treated with 3 μ M Cu8AqN and 5 μ M doxorubicin, while MDA-MB-231 cells were treated with 4.2 μ M Cu8AqN and 20 μ M tBHP. The red fluorescence indicates the presence of ROS. Both cell lines were treated for 6 h. The cells were viewed on an Olympus BX41 epifluorescence microscope at 400x magnification. Images were captured with an Olympus DP72 and were analysed with the ImageJ Software. Scalebar: 20 μ m, AU: arbitrary units.

both cell lines, caspase-9 activation occurred in almost 100% of the cells treated with the Cu8AqN complex and was comparable to that of doxorubicin as shown in Fig. 5C.

3.6. Cu8AqN increased the activity of caspase-7 in MCF-7 cells and caspase-3/7 in MDA-MB-231 cells

The activation of effector caspase-3 and caspase-7 is responsible for nuclear fragmentation. The caspase-3/7 assay indicated that Cu8AqN was able to cause cell death by apoptosis after 48 h as shown in Fig. 6. MCF-7 cells do not express caspase-3 but caspase-7 (Jänicke, 2008). Untreated MCF-7 cells, showed no caspase-7 activity (Fig. 6A, panel a and b) whilst the cells treated with Cu8AqN (Fig. 6A, panel c and d) and doxorubicin (Fig. 6A, panels e and f and Fig. 6B) had 50 % and close to

90% of cells positive for active caspase-7, respectively. Caspase 3/7 activity was absent in untreated MDA-MB-231 cells, (Fig. 6B, panel g and h) whilst Cu8AqN and doxorubicin treated cells had close to 100% of cells with active caspase-3/7 (Fig. 6B, panels i, j, k and l and Fig. 6C).

3.7. Cu8AqN changed the expression levels of apoptotic regulatory proteins in both MCF-7 and MDA-MB-231 breast cancer cells

Following confirmation of Cu8AqN-induced apoptotic cell death, the effects of the Cu8AqN complex on the expression of apoptosis regulatory proteins using a focussed apoptosis proteome array was investigated. MCF-7 cells were treated with 3 μ M of Cu8AqN and the copper-free 8AqN to obtain a direct comparison of the effect of the copper complex and its copper free ligand. MDA-MB-231 cells were treated with

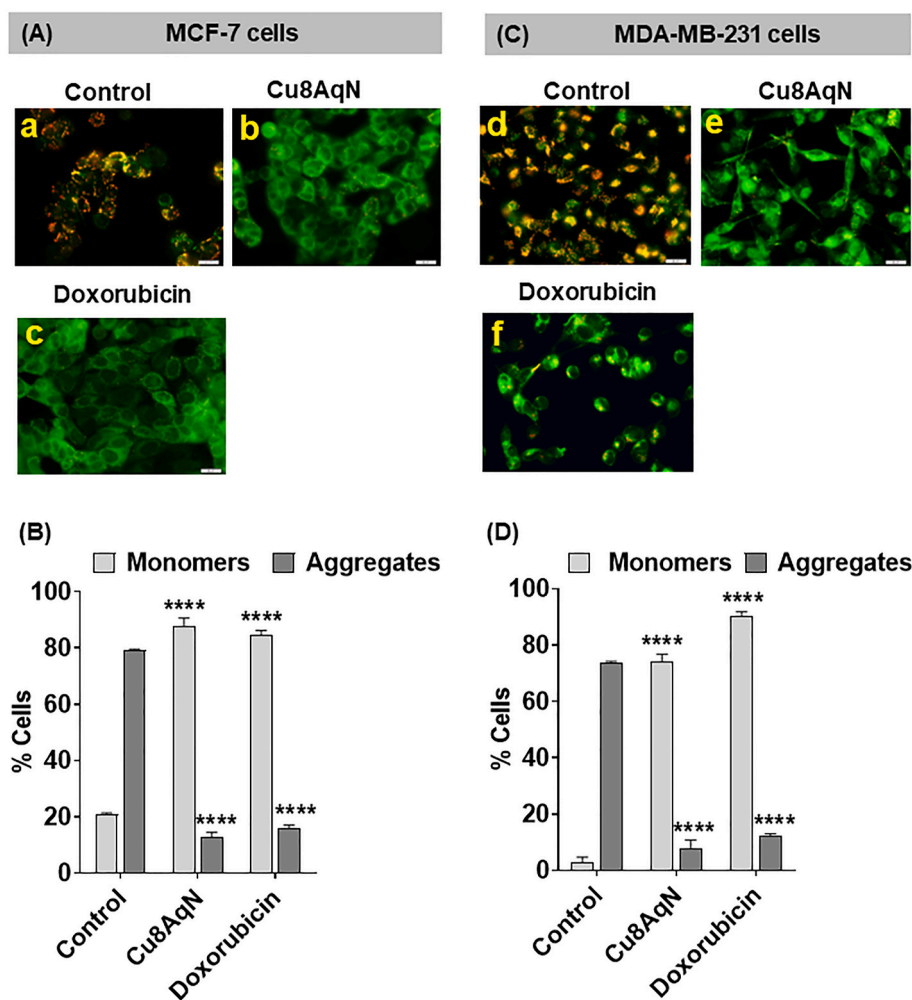


Fig. 4. Cu8AqN caused the loss of mitochondrial membrane potential ($\Delta\Psi_m$) in MCF-7 and MDA-MB-231 cells. MCF-7 cells were treated with 3 μM Cu8AqN and 5 μM doxorubicin, while MDA-MB-231 cells were treated with 4.2 μM Cu8AqN and 10 μM doxorubicin for 18 h. (A and C) are representative fluorescent photomicrographs showing the effects of Cu8AqN and doxorubicin on JC-1 aggregates and monomers in MCF-7 and MDA-MB-231 cells. B and D shows the percentage of JC-1 aggregates and monomers in MCF-7 and MDA-MB-231 cells of three independent experiments. The cells were viewed on an Olympus BX41 epifluorescence microscope. Images were captured with an Olympus DP72 camera and analysed with the Olympus CellSens Software. Magnification: 400x, Scalebar:20 μm .

Cu8AqN at a concentration of 3.1 μM and compared to the effects caused by doxorubicin. Doxorubicin concentrations of 5 μM in MCF-7 cells and 9 μM in MDA-MB-231 cells were used. These concentrations were selected as no obvious changes were observed on the gross morphology of the treated cells were observed by phase contrast microscopy after an 18 h treatment period. Protein expression levels were measured as arbitrary units representing pixel density.

3.7.1. Cu8AqN modulated the expression of apoptotic regulatory proteins in MCF-7 cells

3.7.1.1. Cu8AqN increased the expression on three phosphorylated p53 species in MCF-7 cells. Baseline expression of three phosphorylated species of p53 (S15, S45 and S392) varied in MCF-7 cells with phospho-p53(S15) being low and phospho-p53(S45) and phospho-p53(S392) being moderate as seen in Fig. 7A and B. The Cu8AqN complex and doxorubicin significantly increased ($p < 0.001$) the expression of three phosphorylated p53 species in the cells when compared to their respective untreated cells. In contrast, 8AqN did not cause meaningful changes to the expression of phospho-p53(S15) and phospho-p53(S45) and decreased phospho-p53(S392). Doxorubicin highly significantly increased the three species of phospho-p53, consistent with its known DNA damaging effects.

3.7.1.2. Cu8AqN decreased the expression levels of IAPs in MCF-7 cells. Baseline expression of the IAPs, cIAP1 (cellular inhibitor of apoptosis protein-1) and XIAP (X-linked inhibitor of apoptosis protein) was high in MCF-7 cells with survivin levels being very high as shown in Fig. 7C and D. Cu8AqN highly significantly decreased the expression of cIAP1 and XIAP. Although the expression of survivin was significantly decreased, it was considered less meaningful since the expression level of survivin in Cu8AqN treated cells remained high. Expression of the three IAPs were decreased by the copper free ligand 8AqN, but to a lesser extent than Cu8AqN. Doxorubicin was the most effective suppressor of all three IAPs, and highly significantly decreased expression of all the IAPs by more than 50%.

3.7.1.3. Cu8AqN increased the expression of HMOX-1 and p21 and suppressed the expression of TNFR1 in MCF-7 cells. Baseline expression of the stress response protein HMOX-1 was low and impressively increased by Cu8AqN. The metal free ligand, 8AqN increased HMOX-1 expression less markedly (Fig. 7E and F), albeit statistically significant. The effect of the copper complex and its metal free ligand was in contrast with doxorubicin which caused a statistically significant decrease of HMOX-1 expression.

Baseline expression of p21 was low and highly significantly ($p < 0.001$) increased from a low to a high expression level by Cu8AqN,

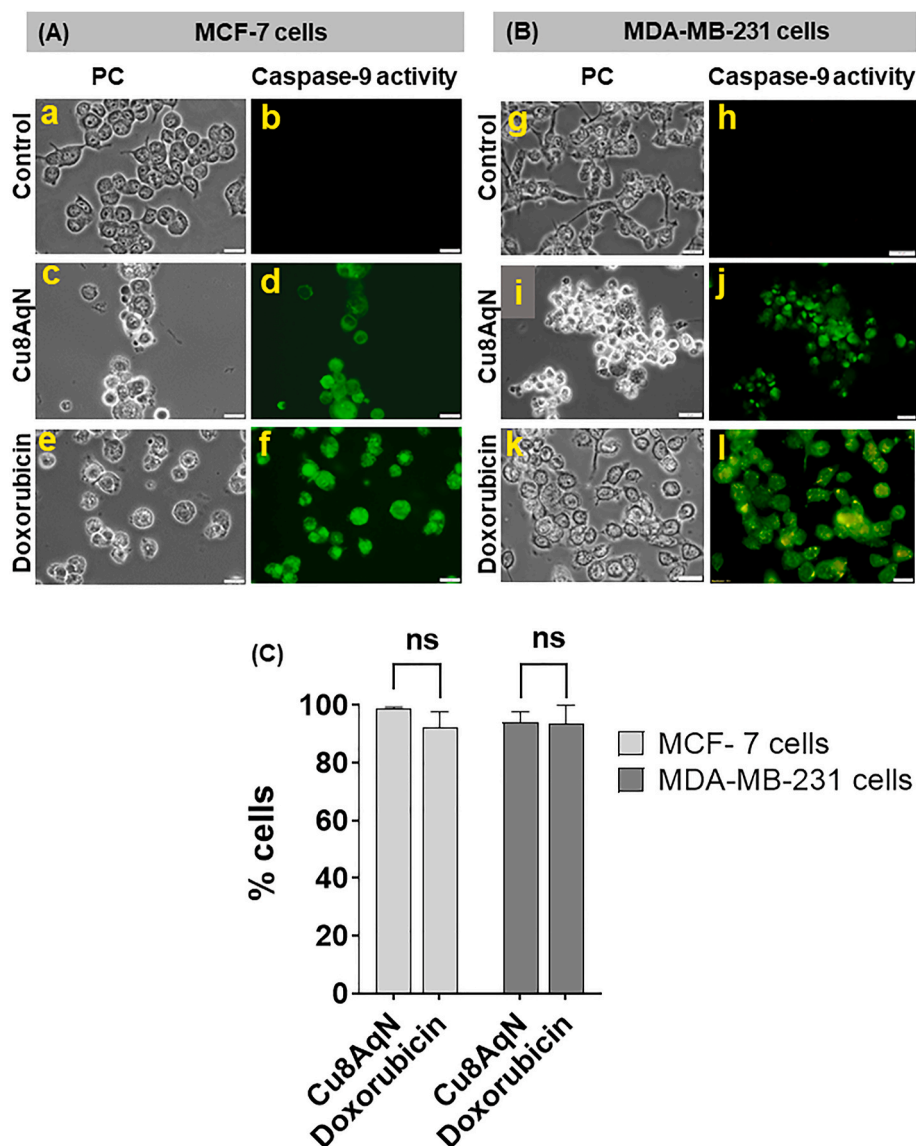


Fig. 5. Cu8AqN and doxorubicin activates caspase-9 in MCF-7 and MDA-MB-231 cells. MCF-7 and MDA-MB-231 cells were treated for 48 h with 3 μ M and 4.2 μ M of Cu8AqN, respectively and doxorubicin at 5 μ M (MCF-7) and 10 μ M (MDA-MB-231). (A) is a representative photomicrograph of MCF-7 cells showing active caspase-9. (B) is a representative photomicrograph showing active caspase-9 in MDA-MB-231 cells. (C) is a bar graph representing the percentage cells with active caspase-9 in MCF-7 and MDA-MB-231 cells of three independent experiments. The cells were viewed on an Olympus BX41 epifluorescence microscope at 400x magnification. Images were captured with an Olympus DP72 camera and analysed with the Olympus CellSens Software. Scalebar: 20 μ m.

whilst the copper free ligand, 8AqN, caused a decrease. This is consistent with the observed increases in phosphorylated p53 species which is known to induce the expression of p21. Doxorubicin caused a statistically significant but poor increase in p21 expression as seen in Fig. 7E and F.

The baseline expression of TNFR1 was high and extensively suppressed by all treatments (Fig. 7E and F). Cu8AqN and doxorubicin significantly decreased ($p < 0.001$) the expression of TNFR1 from high to very low, whilst the 8AqN copper free ligand showed a statistically significant decrease with expression remaining medium high (Fig. 7E and F.)

3.7.1.4. Cu8AqN decreased the expression of HIF-1 α and BAD in MCF-7 cells. The baseline expression of the HMOX-1 transcription factor, HIF-1 α , was high and suppressed by Cu8AqN, 8AqN and doxorubicin. Both 8AqN and doxorubicin were more effective suppressors than Cu8AqN (Fig. 7G and H). The baseline expression of the pro- and anti-apoptotic Bcl-2 related proteins indicated high expression levels of BAD and low

expression of Bcl-2 (Fig. 7G and H). The Cu8AqN, 8AqN and doxorubicin caused a significant decrease in the expression of BAD. Bcl-2 expression was statistically significantly reduced but given its low baseline expression level this was not considered to be meaningful.

3.7.2. Cu8AqN modulated the expression of apoptotic regulatory proteins in MDA-MB-231 cells

3.7.2.1. In MDA-MB-231 cells, Cu8AqN selectively changed expression levels of phosphorylated p53 species. In MDA-MB-231 cells, baseline expression of phospho-p53(S15) and phospho-p53(S392) were moderate, in contrast with the high expression of phospho-p53(S46) (Fig. 8A and B) The treatment of the cells with Cu8AqN caused non-significant changes in the expression of phospho-p53(S15), phospho-p53(S46) and phospho-p53(S392). Doxorubicin however, caused a significant increase in the expression of phospho-p53(S15) and phospho-p53(S392) in the cells, but did not significantly affect the expression levels of phospho-p53(S46) (Fig. 8A and B).

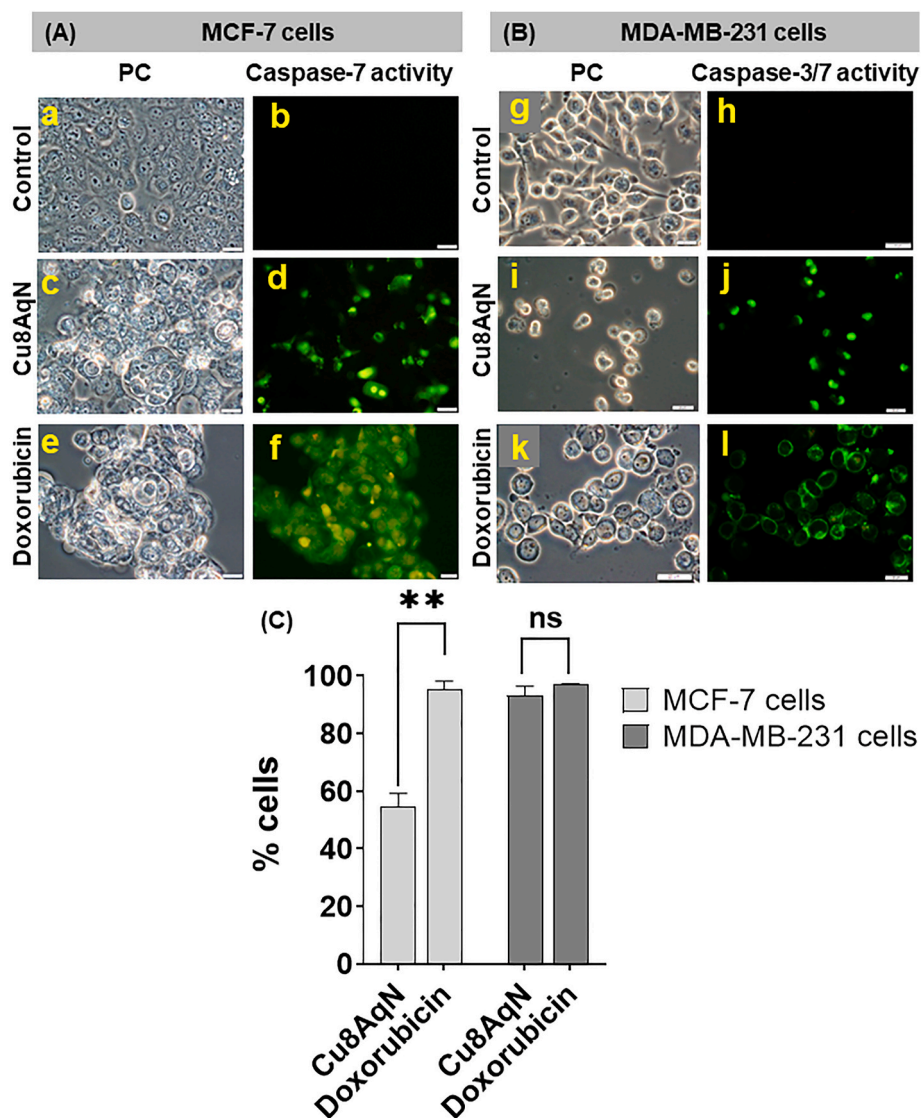


Fig. 6. Representative photomicrographs and bar graphs showing the activation of caspase-7 in MCF-7 cells, and caspase-3/7 in MDA-MB-231 cells. (A) representative photomicrographs of MCF-7 cells showing active caspase-7 cells after treatment with Cu8AqN (3 μ M) and doxorubicin (5 μ M) for 48 h. (B) representative photomicrographs showing active caspase-3/7 in MDA-MB-231 cells after treatment with Cu8AqN (4.2 μ M) and doxorubicin (10 μ M) for 48 h. (C) is a bar graph showing the average percentage of cells with active caspase-3 and caspase-3/7 from three independent experiments. The cells were viewed on an Olympus BX41 epifluorescence microscope at 400x magnification. Images were captured with an Olympus DP72 camera and analysed with the Olympus CellSens Software. Scalebar: 20 μ m.

3.7.2.2. Cu8AqN decreased the expression of IAPs in MDA-MB-231 cells. Baseline expression of cIAP1 was moderately high in MDA-MB-231 cells and significantly suppressed by Cu8AqN and doxorubicin, as shown in Fig. 8C and D. In comparison, doxorubicin was more effective in suppressing cIAP1 than Cu8AqN. XIAP was moderately expressed and was significantly suppressed by both Cu8AqN and doxorubicin. Survivin expression was very high in the cells and significantly suppressed by Cu8AqN. In contrast, doxorubicin increased the expression levels of survivin (Fig. 8C and D).

3.7.2.3. Cu8AqN increased the expression of HMOX1, suppressed the expression of TNFR1 and decreased p21 expression in MDA-MB-231 breast cancer cells. MDA-MB-231 untreated cells had a moderate baseline expression of HMOX-1 expression. HMOX-1 was highly significantly increased ($p < 0.001$) in the cells treated with Cu8AqN and decreased in the cells treated with doxorubicin, Fig. 8E and F. Baseline expression of p21 was low in MDA-MB-231 cells, treatment of the cells with Cu8AqN decreased p21 expression in the cells with poor significance whilst

doxorubicin did not affect the expression of p21 in the cells as seen in Fig. 8E and F. Baseline expression of TNFR1 was medium low and significantly decreased ($p < 0.001$) by Cu8AqN and doxorubicin, the latter causing more suppression than Cu8AqN, as shown in Fig. 8E and F.

3.7.2.4. Cu8AqN decreased the expression of HIF-1 α and BAD in MDA-MB-231 cells. Unlike MCF7 cells the baseline expression of the HMOX-1 transcription factor HIF-1 α was moderate and suppressed by Cu8AqN. From the group of BCL-2 related proteins BAD was the only protein with high baseline expression, which was significantly decreased by Cu8AqN and doxorubicin, similarly to what was observed for MCF-7 cells (Fig. 8G and H). Bcl-2 levels were significantly decreased by Cu8AqN and doxorubicin, but due to the low levels of baseline expression, the decrease was not considered to be meaningful.

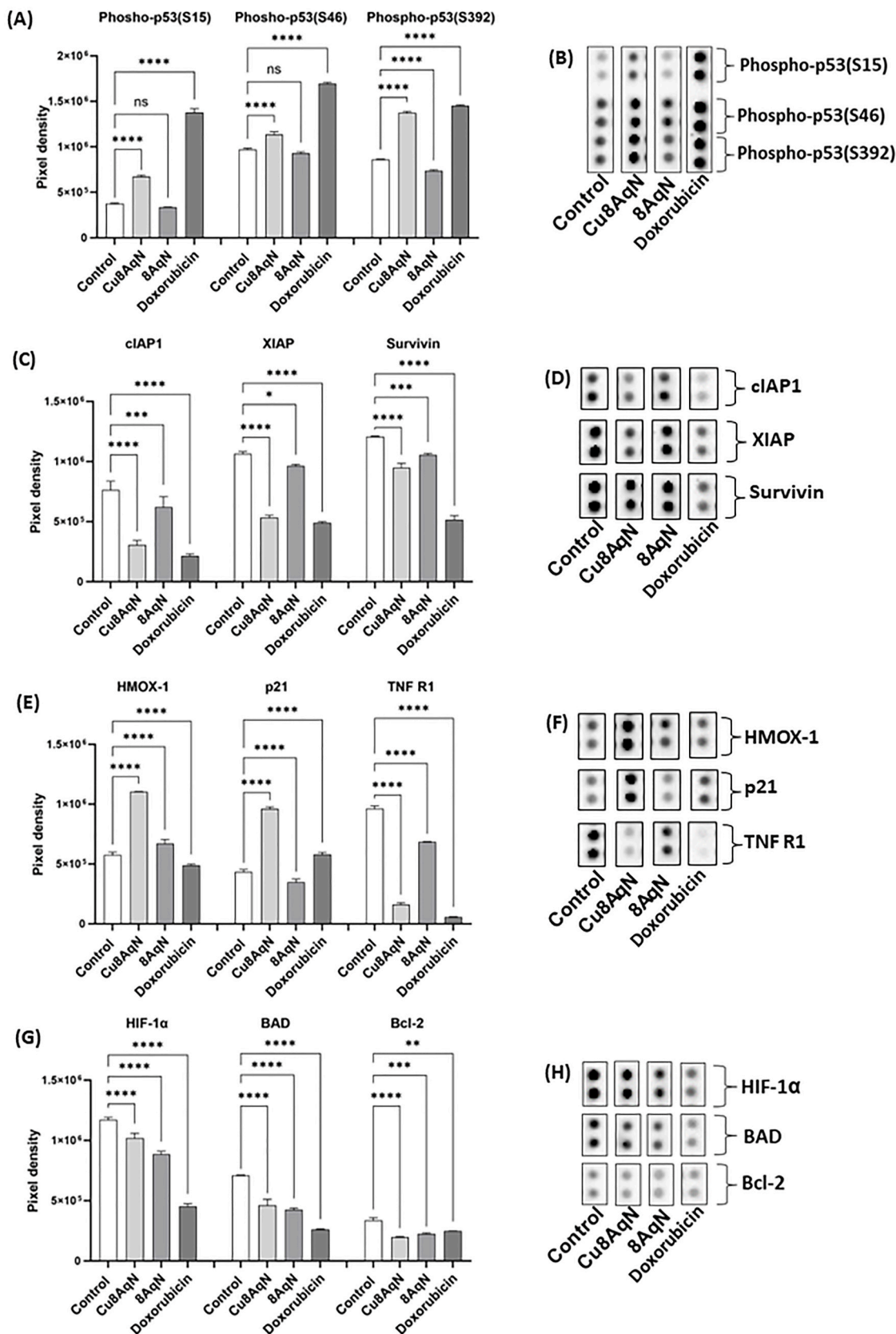


Fig. 7. Cu8AqN caused changes to the expression levels of apoptosis regulatory proteins of MCF-7 breast cancer cells. The figure shows the expression intensity and the segment of the nitrocellulose membrane array with the blots for each protein. The cells were treated with 3 μ M of Cu8AqN, 3 μ M of 8AqN, and 5 μ M of doxorubicin for 18 h. (A) and (B) shows the effects of Cu8AqN, 8AqN and doxorubicin on the expression of phospho-p53(S15), phospho-p53(S46), and phospho-p53(S392). (C) and (D) shows the changes caused by Cu8AqN, 8AqN and doxorubicin on the expression levels of cIAP1, XIAP and survivin. (E) and (F) shows changes in the expression levels of HMOX-1, p21, and TNFR1. (G) and (H) shows the effect on HIF-1, BAD and Bcl-2 in MDA-MB-231 cells.

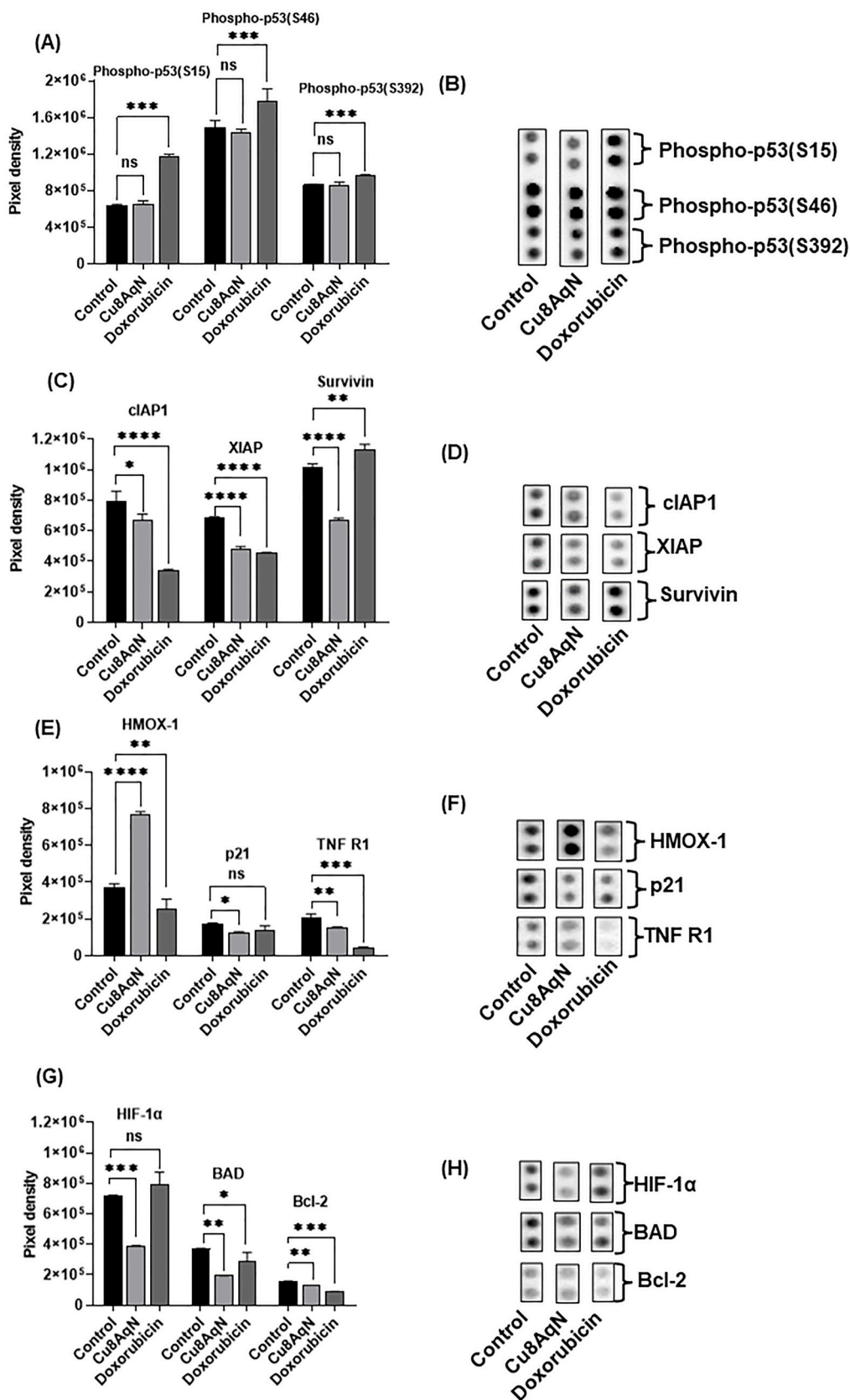


Fig. 8. Cu8AqN caused changes in the expression of apoptosis regulatory proteins in MDA-MB-231 breast cancer cells. The figure shows the expression intensity and the segment of the nitrocellulose membrane array with the blots for each protein. The cells were treated with 3.1 μ M of Cu8AqN and 9 μ M of doxorubicin for 18 h. (A) and (B) shows the effects of Cu8AqN and doxorubicin on the expression of phospho-p53(S15), phospho-p53(S46), and phospho-p53(S392). (C) and (D) illustrates the changes caused by Cu8AqN and doxorubicin on the expression levels of cIAP1, XIAP, and survivin. (E) and (F) shows the changes in the expression levels of HMOX-1, p21, and TNF R1. (G) and (H) shows the effect on HIF-1 α , BAD and Bcl-2 in MDA-MB-231 cells.

3.8. The Cu8AqN complex increased expression of HMOX-1 in MCF-7 and MDA-MB-231 cells

Immunofluorescence confirmed the increased expression of HMOX-1 in both cell lines as shown in (Fig. 9). In untreated MCF-7 cells, HMOX-1 expression was located mainly in the nucleus (Fig. 9A, panel b and c) whilst treatment with Cu8AqN caused HMOX-1 relocation from the nucleus to the cytoplasm (Fig. 9A, panel e and f). In untreated MDA-MB-231 cells (Fig. 9B, panel h and i), HMOX-1 was observed in both the nucleus and cytoplasm. Following treatment with the Cu8AqN, HMOX-1 remained associated with the nucleus in most of the cells with a more intense fluorescence signal (Fig. 9B, panel k and l).

3.9. Cu8AqN increased the expression of p21 in MCF-7 and MDA-MB-231 cells

Expression of p21 was observed in 23.6 % of untreated MCF-7 cells with 6.3 % having an intense fluorescence signal (Table 2 and Fig. 10A, panel a and b). Treatment with Cu8AqN increased the p21 positive cells to 80.6 % with 39.3 % of cells showing an intense p21 signal (Fig. 10A panels c and d, and Table 2). Doxorubicin caused 95.0 % of cells to have a positive signal with 54 % of cells showing an intense p21 signal (Table 2 and Fig. 10A, panels e and f). In contrast, untreated MDA-MB-231 cells did not show p21 expression and Cu8AqN and doxorubicin increased the percentage of cells expressing p21 to 83.3 % and 100%, respectively (Table 2 and Fig. 10B, panels i–l).

3.10. Stability of Cu8AqN in plasma, phosphate buffer, and DMSO

The stability of a metallo-drug candidate is important for several reasons, including whether it will retain its ligand(s) upon interaction with biomolecules and survive intact for a reasonable period in the blood stream in order to reach the intended target site/s. Many metal-drug candidates like NAMI-A (Ru^{2+}), auranofin (Au^+), and cisplatin (Pt^{2+}) undergo ligand exchange reactions and ultimately react as a more simple (ionic) metal species with biomolecules (Van der Westhuizen et al., 2021; Alessio, 2017).

The Cu(II) complex Cu8AqN was stable over prolonged periods in pure DMSO and phosphate buffer at pH 7.5 (Fig. S7). No chemical changes such as bond dissociation or metal ion release could be detected over 36 h in DMSO, which often enhances the dissociation rate of metal complexes (Keller et al., 2020)

The stability of Cu8AqN in human plasma was evaluated *in vitro* as a function of time by spectroscopy in the UV–visible region (Fig. 11). The

Table 2

Percentage of MCF-7 and MDA-MB-231 cells expressing p21 following treatment with Cu8AqN and doxorubicin for 18 h.

MCF-7 cells			
Treatment	High intensity p21 expression (%)	Low intensity p21 expression (%)	Total p21 expression (%)
Control	6.3 ± 1.5	17.3 ± 2.5	23.6 ± 5.6
Cu8AqN	39.3 ± 13.54	41.3 ± 9.29	80.6 ± 22.7
Doxorubicin	54.0 ± 4.7	41.0 ± 3.5	95.0 ± 8.1
MDA-MB-231 cells			
Treatment	High intensity p21 expression (%)	Low intensity p21 expression (%)	Total p21 expression (%)
Control	0.00	0.00	0.00
Cu8AqN	40.0 ± 9.8	43.3 ± 8.2	83.3 ± 18.0
Doxorubicin	38.0 ± 5.6	62.0 ± 8.8	100.0 ± 14.4

spectral changes showed that the 480 nm ($\pi \rightarrow \pi^*$) band of Cu8AqN and its vibronic component at 450 nm both decreased in intensity over time with a negligible change in wavelength. The band at 362 nm decreased in intensity and shifted to 372 nm after 8 h, while a new band peaking at 402 nm increased in intensity over the same period. The spectral changes were accompanied by two discrete isosbestic points at 379 and 425 nm. This single pair of isosbestic points remained unchanged throughout the reaction, suggesting a simple chemical conversion operating in a single step, i.e., reactant \rightarrow product(s). The kinetics of the reaction (monitored at 484 nm) indicated that the process was first order ($t_{1/2} = 6.2 \pm 0.2$ h) as shown in Fig. 11. This is comparable to that reported for paclitaxel, an approved cancer drug, which has a plasma half-life of 6.54 ± 1.43 h (Brouwer et al., 2000). Since weak absorption bands commensurate with the presence of Cu(II), remained present in the 540–650 nm region of the spectrum after ~ 1.5 half-lives (9 h), reductive demetallation of the copper complex to form colourless Cu(I), seemed unlikely (Fig. S9). The data suggested a simple exchange of the Cu(II) ion to release the Schiff base ligand, 8AqN. After 24 h, only 6% of the initial absorption intensity remained. The main spectral peaks prevalent at 9 h in the reaction were nevertheless still observed after 24 h (albeit with significantly diminished amplitude). Furthermore, the broad, overlapping weaker-intensity bands due to Cu(II) at 545 and 568 nm were

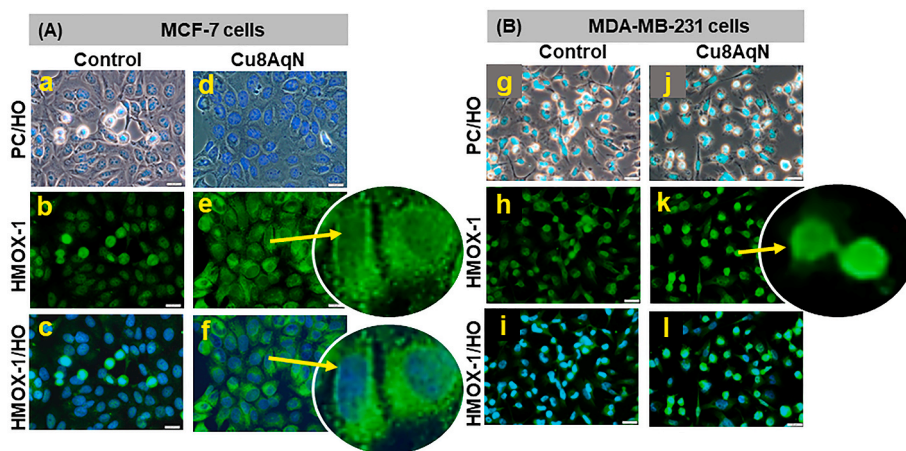


Fig. 9. Immunofluorescence images showing the increased expression of HMOX-1 in MCF-7 and MDA-MB-231 cells. (A) shows HMOX-1 in MCF-7 cells and B shows HMOX-1 in MDA-MB-231 cells. MCF-7 and MDA-MB-231 cells were treated with Cu8AqN at 3 μM and 3.1 μM , respectively and doxorubicin was used at 5 μM in MCF-7 cells and 9 μM in MDA-MB-231 cells for an 18 h treatment period. The cells were viewed with an Olympus BX41 epifluorescence microscope, images were captured with an Olympus DP72 camera and analysed with the Olympus CellSens Software. Magnification: 400x. Scalebar: 20 μm .

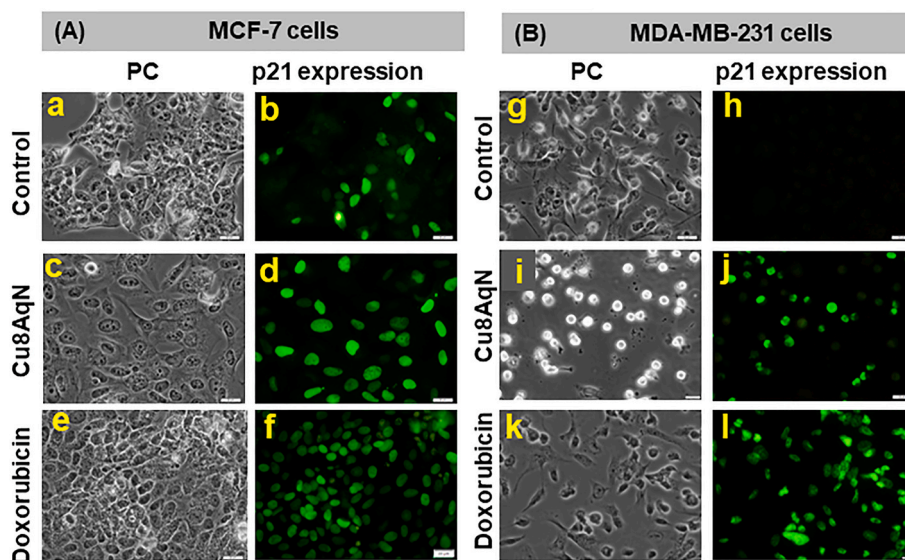


Fig. 10. Photomicrographs showing the increased expression of p21 in MCF-7 and MDA-MB-231 cells following treatment with Cu8AqN and doxorubicin. (A) MCF-7 cells treated with 3 μM Cu8AqN and 5 μM doxorubicin and (B) MDA-MB-231 cells treated with Cu8AqN at 3.1 μM and doxorubicin 9 μM for 18 h. The cells were viewed with an Olympus BX41 epifluorescence microscope, images captured with an Olympus DP72 camera and analysed with the Olympus CellSens Software. Magnification:400x. Scalebar: 20 μm .

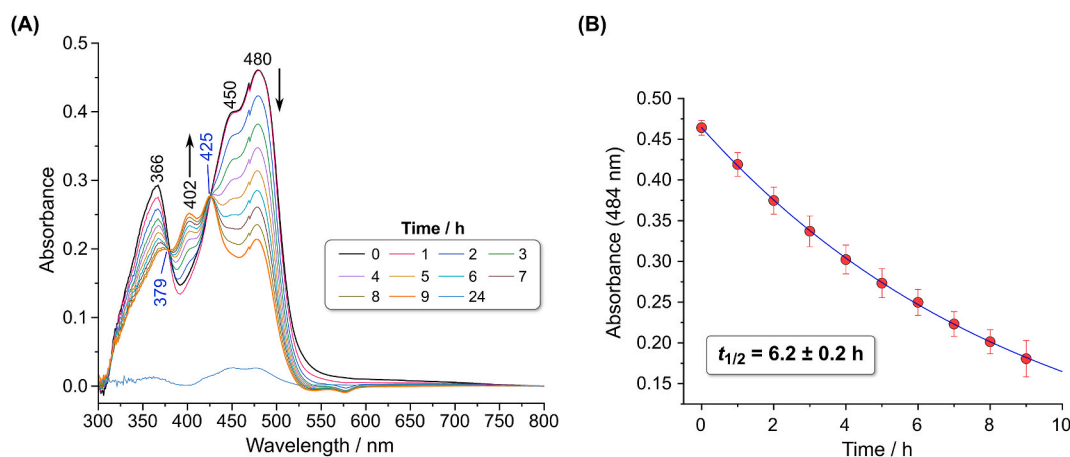


Fig. 11. Stability of Cu8AqN measured in human plasma. (A) UV-visible spectral changes for Cu8AqN (63 μM) recorded in a solution of human blood plasma diluted with phosphate buffer (50 mM KH_2PO_4 , pH 7.50, 1:4 ratio) as a function of time. Peak maxima and isosbestic points are indicated in black and blue typeface, respectively. (B) Nonlinear least-squares regression fit of the absorbance decay curve to a single exponential function (rate constant, $k = 0.111 \pm 0.004 \text{ h}^{-1}$; half-life, $t_{1/2} = 6.2 \pm 0.2 \text{ h}$; $\chi^2 = 0.00762$; $R^2 = 0.9999$).

better resolved after 24 h (Fig. S9).

In summary; our *in vitro* kinetics study in diluted human plasma showed that the decay of Cu8AqN was monophasic with a plasma half-life of $6.2 \pm 0.2 \text{ h}$ at 37 $^\circ\text{C}$. In addition, the spectroscopic data of Fig. 11 suggest that Cu8AqN was not reductively de-metallated via a Cu(I) intermediate because signals from Cu(II) alone are evident after 24 h, i.e., bands at 545 nm and 568 nm due to d-d electronic transitions for chelated Cu^{2+} are present, (Fig. S9). A possible explanation for this observation is that Cu(II) was released from the Schiff base ligand 8AqN (see Figs. S8 and S10) and subsequently bound to the high-affinity Cu(II) transporter motif (the N-terminal Asp-Ala-His tripeptide) of human serum albumin (Laussac and Sarkar, 1984; Bal et al., 1998; Hureau et al., 2011).

4. Discussion

4.1. Cu8AqN is an effective inhibitor of breast cancer cell proliferation and induces intrinsic apoptosis

Cu8AqN showed selective toxicity towards MCF-7 and MDA-MB-231 breast cancer cells with IC_{50} values below 5 μM , compared to almost 10 μM for normal MCF-10A cells. The increased IC_{50} value of the normal cells line, MCF-10A, indicates some selectivity towards cancer cells. The copper free ligand, 8AqN was poorly active in both cancer cell lines indicating that copper increased the cytotoxicity of the ligand. The IC_{50} values compared favourably to doxorubicin, a commonly used cancer treatment. Doxorubicin did not show selectivity towards the cancer or normal cells and was poorly active against triple negative MDA-MB-231 cells.

Fragmentation and condensation of the nuclei, typical apoptotic characteristics, (Galluzzi et al., 2018) indicated Cu8AqN caused

apoptotic cell death in both cell lines. Doxorubicin, a known inducer of apoptosis, showed similar effects (Wang et al., 2004). The absence of red stained PI nuclei in Cu8AqN treated cells indicated the absence of overt necrosis (Atale et al., 2014). 8AqN, did not cause noticeable morphological changes at the concentrations tested, confirming its lack of efficacy.

An increase in annexin V binding to phosphatidylserine confirmed apoptotic cell death. Phosphatidylserine translocate to the outer leaflet of the cell membrane during apoptosis (Crowley et al., 2016). The Cu8AqN treated MCF-7 cells were primarily early apoptotic whilst late apoptotic cells were present in MDA-MB-231 cells, indicating a faster response and greater sensitivity to the copper complex.

The increased activity of caspase-3/7 in MDA-MB-231 and increased caspase-7 activity in MCF-7 cells following treatment with Cu8AqN confirmed apoptotic cell death. Caspase-3/7 activation causes cell shrinkage, membrane blebbing, nuclear fragmentation and condensation leading to apoptosis (Olsson and Zhivotovsky, 2011). MCF-7 cells do not express caspase-3, with caspase-7 being the primary effector caspase (Jänicke, 2008).

The formation of ROS commonly occurs with cancer drugs and is associated with the induction of intrinsic apoptosis. Various copper complexes increase ROS formation and apoptosis in cell lines representing different cancers (Harmse et al., 2019; Li et al., 2019; Zehra et al., 2021b). Cu8AqN increased ROS in both MCF-7 and MDA-MB-231 cells with superior activity in MDA-MB-231 cells most likely promoting mitochondrial dysfunction.

The loss of mitochondrial membrane potential and the activation of caspase-9 are essential for the formation of the apoptosome and activation of the intrinsic apoptotic pathway (Galluzzi et al., 2018) Cu8AqN and doxorubicin caused the loss of mitochondrial membrane integrity in both cell lines causing leakage of cytochrome *c* and pro-apoptotic factors like Smac/Diablo and HTRA(OM) from the mitochondria. Cu8AqN and doxorubicin were effective activators of caspase-9 in both cell lines confirming activation of intrinsic apoptosis. In addition, the failure of Cu8AqN and doxorubicin to activate caspase-8 and the loss of TNFR1 expression in both cell lines confirmed that the extrinsic apoptotic pathway was not activated.

4.2. Cu8AqN modulated the expression of important apoptotic related proteins including p53, IAPs, p21 and HMOX-1

The *TP53* tumour suppressor gene encodes the p53 tumour suppressor and is frequently mutated in breast and other cancers (Dumay et al., 2013). MDA-MB-231 triple negative breast cancer cells have a missense mutation of *TP53* while MCF-7 are wild type *TP53* expressing cells (Alkhalaf and El-Mowafy, 2003).

In MDA-MB-231 cells Cu8AqN decreased the expression of phospho-p53(S46) but not phospho-p53(S15), and phospho-p53(S392). Baseline phospho-p53(S46) expression was very high and the observed decrease in suppression is therefore not considered to have a profound effect on the cells. Doxorubicin increased the expression of phospho-p53(S15), and caused small increases of phospho-p53(S46) and phospho-p53(S392) suggesting inhibition of p53 degradation. In MCF-7 cells, Cu8AqN increased the expression levels of all three phosphorylated p53 species whilst the 8AqN ligand had no effect. A similar but more pronounced increase was observed for doxorubicin. Accumulation of the phosphorylated species of p53 indicates DNA damage and activation of DNA repair. In normal cells with wild type p53, its levels are low due to proteasomal degradation by MDM2 (Junttila and Evan, 2009). Upon DNA damage or cell stress, p53 is phosphorylated, accumulates in the cell and translocate to the nucleus to transactivate genes involved in the initiation of apoptosis and/or DNA repair as well as the tumour suppressor gene p21 (Duffy et al., 2022).

Unlike wild type p53, mutant p53 protein loses its tumour suppressive function and may acquire gain of function mutations leading to tumour progression and chemoresistance (Dumay et al., 2013; Yue et al.,

2017; Marvalim et al., 2023). Mutant p53 bypasses MDM2 mediated proteasomal degradation and is present at high levels in cancer cells (Muller and Vousden, 2013). Changes to the expression levels of mutant p53 was observed with other copper complexes and the MDA-MB-231 cell line, (Lee et al., 2021), and in HT29 colorectal cancer cells where the high baseline expression of mutant p53 was suppressed (Harmse et al., 2019).

The proteome array data indicated that Cu8AqN treatment of both cell lines caused a profound increase in the protein expression level of HMOX-1. HMOX-1, is an inducible stress response protein, and is expressed in many cancers, including breast cancer (Podkalicka et al., 2018; Gandini et al., 2019). The exact role of HMOX-1 in breast cancer, whether promoting cancer cell survival or cell death remains unclear (Noh et al., 2013; Luu-Hoang et al., 2021). The increase in HMOX-1 observed with the proteome array was confirmed by an increase of immunofluorescence in both cell lines. HMOX-1 was primarily localized to the nucleus in untreated control cells. In MDA-MB-231 cells, the Cu8AqN induced increase was localized to the nucleus whilst in MCF-7 the increase was observed in the cytoplasm. Nuclear HMOX-1 is truncated, enzymatically inactive and associated with more aggressive tumours where it is thought to act as a cofactor in gene transcription (Biswas et al., 2014; Hsu et al., 2017). Cytoplasmic HMOX-1 is assumed to be enzymatically active and required for the normal cell survival response to oxidative stress (Gandini et al., 2019). The implications of increased HMOX-1 expression in breast cancer requires further investigation.

The transcription of the *HMOX-1* gene is regulated by various transcription factors including HIF-1 α , nuclear factor erythroid 2-related factor-2 (Nrf2), and activator protein 1(AP-1) (Loboda et al., 2016) Protein array data indicated high baseline expression of HIF-1 α in MCF-7 and MDA-MB-231 cell lines. Cu8AqN and doxorubicin decreased levels of HIF-1 α in MCF-7 cells, whereas in MDA-MB-231 cells Cu8AqN decreased and doxorubicin conversely increased HIF-1 α expression. This poor correlation suggests that other HMOX-1 transcription factors were responsible for the increased HMOX-1 levels in MDA-MB-321 cells.

High expression levels of cIAP1, XIAP, and survivin are associated with cancer progression, chemoresistance and increased morbidity (Fulda, 2014; Finlay et al., 2017). Cu8AqN decreased cIAP1, XIAP, and survivin in both MCF-7 and MDA-MB-231 cells, creating a pro-apoptotic environment. XIAP and cIAP1 inhibits caspase-3/7, whilst survivin inhibits caspases by binding to the catalytic domain of caspase-3, -7 and -9 via its BIR domains (Fulda, 2014; Finlay et al., 2017). The suppression of cIAP1, XIAP and survivin aligns with increased caspase-9 and caspase-3/7 activity, promoting apoptosis.

BAD, a member of the Bcl-2 family of proteins, interacts with Bcl-2 and translocate BAX to the mitochondria, thereby increasing mitochondrial membrane permeability and the release of cytochrome *c*. BAD function is controlled by phosphorylation at serine-112, -115 and -136 via PKA/MAPK and AKT pathways. Increased levels of phosphorylated BAD are associated with resistance to apoptosis (Bui et al., 2018; Boac et al., 2019). Cu8AqN and doxorubicin decreased BAD expression in both cell lines. This effect may be associated with the copper free ligand, 8AqN, which suppressed BAD in a similar manner to Cu8AqN in MCF-7 cells. Given the dual role of BAD in apoptosis, further studies to determine the effects of Cu8AqN on the various phosphorylated forms of BAD are warranted.

An evaluation of Bcl-2 and Bax showed low baseline expression in MCF-7 and MDA-MB-321 cells, which was statistically significantly decreased by Cu8AqN. Given the low expression levels of these proteins their suppression was not considered to have a meaningful role.

p21 is a cyclin-dependent kinase inhibitor and its expression is upregulated by p53 in response to DNA damage or oxidative stress (Shamloo and Usluer, 2019). Activation of the p53 response, as in MCF-7 cells, caused the transcription of p21 which inhibited cyclin dependent kinases preventing the completion of the cell cycle (Georgakilas et al., 2017). The function of p21 depends on its subcellular

localization (Zhang et al., 2000). Cytoplasmic p21 prevents apoptosis by binding and preventing the activation of pro-caspase-3, and caspase-8 (Karimian et al., 2016; Georgakilas et al., 2017). Nuclear p21 inhibits cyclin dependent kinase-2 and -4, and binds to PCNA, thereby preventing progression of the cell cycle from the G1 to the S phase (Shamloo and Usluer, 2019). In untreated MCF-7 cells, immunofluorescence indicated low baseline expression of p21 in the nucleus and an increase of nuclear p21 expression after Cu8AqN and doxorubicin treatment. This was mirrored by the proteome array data which showed that copper free 8AqN did not affect p21 expression. In MDA-MB-231 cells immunofluorescence data showed increases in p21 expression similar to that of MCF-7 cells with increased intensity localized to the cell nucleus.

4.3. Cu8AqN is sufficiently stable in human plasma

The stability of Cu8AqN in human plasma, is of direct relevance to its longer-term prospects as a potential drug candidate (Sarpong-Kumankomah and Gailer, 2021). Our *in vitro* kinetics study with human plasma indicated a plasma half-life for Cu8AqN of approximately 6 h at 37 °C, which is comparable to paclitaxel, a widely used chemotherapeutic drug (Brouwer et al., 2000). Importantly, the decrease in Cu8AqN concentration was monophasic, indicating the slow dissociation of Cu (II) from Cu8AqN which would allow the intact complex to enter cells.

5. Conclusion

The cellular mechanism of cytotoxicity induced by a Cu(II) complex of a quinoline-containing Schiff base chelate, Cu8AqN, was investigated. The data indicate that Cu8AqN selectively targeted breast cancer cells at clinically relevant, low micromolar concentrations. Cell death occurred via the activation of the intrinsic apoptotic pathway due to the suppression of apoptotic inhibitory proteins. The combination of suppression of IAP's and increased p21 expression created a pro-apoptotic environment promoting cell death. The ability of the complex to induce the expression of HMOX-1 must be further investigated to determine the impact of this on cell survival. The effects observed in triple negative MDA-MB-231 cells are particularly encouraging. An *in vitro* study with human plasma indicated a half-life of 6.2 ± 0.2 h for Cu8AqN. This study provides valuable insights in the response of cancer cells to Cu8AqN illustrating the potential benefits of copper complexes in cancer treatment.

Funding

This work was supported by the University of the Witwatersrand Faculty of Health Science Research Committee and the McGill Bequest to the Pharmacology Division. NM was supported by the PhD Innovation grant of the Nation Research Foundation, Pretoria (South Africa) This work is also based on research supported by the South African Research Chairs Initiative of the Department of Science and Innovation (DSI) and National Research Foundation (NRF) of South Africa (Grant No 64799, OQM).

CRediT authorship contribution statement

Nonzuzo Myeza: Writing – review & editing, Writing – original draft, Investigation, Formal analysis, Data curation. **Cathy Slabber:** Writing – review & editing, Validation, Methodology, Formal analysis, Data curation. **Orde Q. Munro:** Writing – review & editing, Methodology, Formal analysis, Conceptualization. **Sheldon Sookai:** Data curation, Formal analysis. **Savannah C. Zacharias:** Data curation. **Carla Martins-Furness:** Writing – review & editing, Formal analysis, Data curation. **Leonie Harmse:** Writing – review & editing, Writing – original draft, Validation, Supervision, Resources, Funding acquisition, Formal analysis, Data curation, Conceptualization.

Declaration of competing interest

None.

Data availability

Data will be made available on request.

List of Abbreviations

IAPs	Inhibitor of apoptosis proteins
AU	Arbitrary Units
Bcl-2	B-cell lymphoma-2 protein
ciAP1	Cellular inhibitor of apoptosis protein-1
h	hour/hours
HIF-1alpha	Hypoxia inducing factor-1α
HMOX-1	Heam oxygenase 1
HTRA (OMI)	High temperature requirement protein A2
HO	Hoechst 33342
MDM2	Mouse double minute 2 homolog
Min	minutes
NF-κB	Nuclear factor kappa B
Smac/Diablo	Second mitochondria-derived activator of caspase
TNFR1	Tumor necrosis factor receptor 1
XIAP	X-linked inhibitor of apoptosis protein
PCNA	Proliferating cell nuclear antigen
PC	Phase contrast
tBHP	Tert-Butyl hydroperoxide

Appendix A. Supplementary data

Supplementary data to this article can be found online at <https://doi.org/10.1016/j.ejphar.2024.176764>.

References

- Aguilar-Jiménez, Z., González-Ballesteros, M., Dávila-Manzanilla, S.G., Espinoza-Guillén, A., Ruiz-Azuara, L., 2022. Development and *in vitro* and *in vivo* evaluation of an antineoplastic copper(II) compound (Casiopaina III-ia) loaded in nonionic vesicles using quality by design. *Int. J. Mol. Sci.* 23 (21), 12756 <https://doi.org/10.3390/ijms232112756>.
- Alessio, E., 2017. Thirty years of the drug candidate NAMI-A and the myths in the field of ruthenium anticancer compounds: a personal perspective. *Eur. J. Inorg. Chem.* 2017, 1549–1560. <https://doi.org/10.1002/ejic.201600986>.
- Ali, A., Banerjee, S., Kamaal, S., Usman, M., Das, N., Afzal, M., Alarifi, A., Sepay, N., Roy, P., Ahmad, M., 2021. Ligand substituent effect on the cytotoxicity activity of two new copper(ii) complexes bearing 8-hydroxyquinoline derivatives: validated by MTT assay and apoptosis in MCF-7 cancer cell line (human breast cancer). *RSC Adv.* 11 (24), 14362–14373. <https://doi.org/10.1039/d1ra00172h>.
- Alkhalaf, M., El-Mowafy, A.M., 2003. Overexpression of wild-type p53 gene renders MCF-7 breast cancer cells more sensitive to the antiproliferative effect of progesterone. *J. Endocrinol.* 179 (1), 55–62. <https://doi.org/10.1677/joe.0.1790055>.
- Atale, N., Gupta, S., Yadav, U.C.S., Rani, V., 2014. Cell-death assessment by fluorescent and nonfluorescent cytosolic and nuclear staining techniques. *J. Microsc.* 255 (1), 7–19. <https://doi.org/10.1111/jmi.12133>.
- Bal, W., Christodoulou, J., Sadler, P.J., Tucker, A., 1998. Multi-metal binding site of serum albumin. *J. Inorg. Biochem.* 70, 33–39. [https://doi.org/10.1016/S0162-0134\(98\)00010-5](https://doi.org/10.1016/S0162-0134(98)00010-5).
- Balsa, L.M., Baran, E.J., León, I.E., 2023. Copper complexes as antitumor agents: *in vitro* and *in vivo* evidence. *Curr. Med. Chem.* 30 (5), 510–557. <https://doi.org/10.2174/0929867328666211117094550>.
- Biswas, C., Shah, N., Muthu, M., La, P., Fernando, A.P., Sengupta, S., Yang, G., Dennery, P.A., 2014. Nuclear heme oxygenase-1 (HO-1) modulates subcellular distribution and activation of Nrf2, impacting metabolic and anti-oxidant defenses. *J. Biol. Chem.* 289 (39), 26882–26894. <https://doi.org/10.1074/jbc.M114.567685>.
- Boac, B.M., Abbasi, F., Ismail-Khan, R., Xiong, Y., Siddique, A., Park, H., Han, M., Saeed-Vafa, D., Soliman, H., Marchion, D.C., 2019. Expression of the BAD pathway is a marker of triple-negative status and poor outcome. *Sci. Rep.* 9 (1), 1–14. <https://doi.org/10.1038/s41598-019-53695-0>.
- Brouwer, E., Verweij, J., Bruijn, P.D., Loos, W.J., Pillay, M., Buijs, D., Sparreboom, A., 2000. Measurement of fraction unbound paclitaxel in human plasma. *Drug Metab. Dispos.* 28, 1141–1145.
- Bui, N.L.C., Pandey, V., Zhu, T., Ma, L., Basappa, L., Lobie, P.E., 2018. BAD phosphorylation as a target of inhibition in oncology. *Cancer Lett.* 415, 177–186. <https://doi.org/10.1016/j.canlet.2017.11.017>.

- Crowley, L.C., Marfell, B.J., Scott, A.P., Waterhouse, N.J., 2016. Quantitation of apoptosis and necrosis by annexin V binding, propidium iodide uptake, and flow cytometry. *Cold Spring Harb. Protoc.* 2016 (11), 953–957. <https://doi.org/10.1101/pdb.prot087288>.
- Dam, J., Ismail, Z., Kurebwa, T., Gangat, N., Harmse, L., Marques, H.M., Lemmerer, A., Bode, M.L., de Koning, C.B., 2017. Synthesis of copper and zinc 2-(pyridin-2-yl)imidazo[1,2-a]pyridine complexes and their potential anticancer activity. *Eur. J. Med. Chem.* 126, 353–368. <https://doi.org/10.1016/j.ejmech.2016.10.041>.
- Duffy, M.J., Synnott, N.C., O'Grady, S., Crown, J., 2022. Targeting p53 for the treatment of cancer. *Semin. Cancer Biol.* 79, 58–67. <https://doi.org/10.1016/j.semcancer.2020.07.005>.
- Dumay, A., Feugeas, J.P., Wittmer, E., Lehmann-Che, J., Bertheau, P., Espié, M., Plassa, L.F., Cottu, P., De Thé, H., 2013. Distinct tumor protein p53 mutants in breast cancer subgroups. *Int. J. Cancer Res.* 132 (5), 1227–1231. <https://doi.org/10.1002/ijc.27767>.
- Emens, L.A., Loi, S., 2023. Immunotherapy approaches for breast cancer patients in 2023. *Cold Spring Harb. Perspect. Med.* 13 (4), a041332. <https://doi.org/10.1101/cshperspect.a041332>.
- Facchetti, G., Ferri, N., Lupo, M.G., Giorgio, L., Rimoldi, I., 2019. Monofunctional PII complexes based on 8-aminoquinoline: synthesis and pharmacological characterization. *Eur. J. Inorg. Chem.* (29), 3389–3395. <https://doi.org/10.1002/ejic.201900644>.
- Finlay, D., Teriete, P., Vamos, M., Cosford, N.D.P., Vuori, K., 2017. Inducing death in tumor cells: roles of the inhibitor of apoptosis proteins. *F1000research* 6, 1–18. <https://doi.org/10.12688/f1000research.10625.1>.
- Fulda, S., 2014. Molecular pathways: targeting inhibitor of apoptosis proteins in cancer—from molecular mechanism to therapeutic application. *Clin. Cancer Res.* 20 (2), 289–295. <https://doi.org/10.1158/1078-0432.CCR-13-0227>.
- Foo, J.B., Low, M.L., Lim, J., Lor, Y., Zainol, A., Eh Dam, V., Napsiah, A., Saiful Yazan, L., 2018. Copper complex derived from S-benzylthiocarbamate and 3-acetylcoumarin induced apoptosis in breast cancer cell. *Biometals* 31 (4), 505–515. <https://doi.org/10.1007/s10534-018-0096-4>.
- Galluzzi, L., Vitale, I., Aaronson, S.A., Abrams, J.M., Adam, D., Agostinis, P., Alnemri, E. S., Altucci, L., Kroemer, G., 2018. Molecular mechanisms of cell death: recommendations of the nomenclature committee on cell death 2018. *Cell Death Differ.* 25 (3), 486–541. <https://doi.org/10.1038/s41418-017-0012-4>.
- Gandini, N.A., Alonso, E.N., Fermento, M.E., Mascaró, M., Abba, M.C., Coló, G.P., Arév, J., Ferronato, M.J., Facchinetti, M.M., 2019. Heme oxygenase-1 has an antitumor role in breast cancer. *Antioxidants Redox Signal.* 30 (18), 2030–2049. <https://doi.org/10.1089/ars.2018.7554>.
- Georgakilas, A.G., Martin, O.A., Bonner, W.M., 2017. p21: a two-faced genome guardian. *Trends Mol. Med.* 23 (4), 310–319. <https://doi.org/10.1016/j.molmed.2017.02.001>.
- Gordon, A.T., Abosedo, O., Ntsimango, S., Hosten, E.C., Myeza, N., Van Eyk, A., Harmse, L., Ogunlaja, A., 2022. Synthesis and anticancer evaluation of copper(II)- and manganese (II)-theophylline mixed ligand complexes. *Polyhedron* 214, 115647. <https://doi.org/10.1016/j.poly.2022.115649>.
- Harbeck, N., 2022. Neoadjuvant and adjuvant treatment of patients with HER2-positive early breast cancer. *Breast* 62 (Suppl. 1), S12–S16. <https://doi.org/10.1016/j.breast.2022.01.006>.
- Harmse, L., Gangat, N., Martins-Furness, C., Dam, J., De Koning, C.B., 2019. Copper-imidazo[1,2-a]pyridines induce intrinsic apoptosis and modulate the expression of mutated p53, haem oxygenase-1 and apoptotic inhibitory proteins in HT-29 colorectal cancer cells. *Apoptosis* : Int. J. Program. Cell Death. 24 (7–8), 623–643. <https://doi.org/10.1007/s10495-019-01547-7>.
- Harmse, L., Dahan-Farkas, N., Panayides, J.L., Van Otterlo, W., Penny, C., 2015. Aberrant apoptotic response of colorectal cancer cells to novel nucleoside analogues. *PLoS One* 10 (9). <https://doi.org/10.1371/journal.pone.0138607>.
- Hsu, F.F., Chiang, M.T., Li, F.A., Yeh, C.T., Lee, W.H., Chau, L.Y., 2017. Acetylation is essential for nuclear heme oxygenase-1-enhanced tumor growth and invasiveness. *Oncogene* 36 (49), 6805–6814. <https://doi.org/10.1038/ncr.2017.294>.
- Hureau, C., Eury, H., Guillot, R., Bijani, C., Sayen, S., Solari, P., Guillon, E., Faller, P., Dorlet, P., 2011. X-ray and solution structures of Cu^{II} GHK and Cu^{II} DAHK complexes: influence on their redox properties. *Chem. Eur J.* 17, 10151–10160. <https://doi.org/10.1002/chem.201100751>.
- Ismail, Z., Dam, J., Penny, C., de Koning, C.B., Harmse, L., 2022. Copper-imidazo[1,2-a]pyridines differentially modulate pro- and anti-apoptotic protein and gene expression in HL-60 and K562 leukaemic cells to cause apoptotic cell death. *Biochim. Biophys. Acta Mol. Cell Res.* 1869 (1), 119160 <https://doi.org/10.1016/j.bbmr.2021.119160>.
- Joshi, H., Press, M.F., 2018. The breast: comprehensive management of benign and malignant diseases. In: Bland, K.I., Copeland, E.M., Klimberg, V.S., Gradishar, W.J. (Eds.), *Molecular Oncology of Breast Cancer*, fifth ed. Elsevier Inc, pp. 282–307. <https://doi.org/10.1016/B978-0-323-35955-9.00022-2> (Chapter 22).
- Jänicke, R.U., 2008. MCF-7 breast carcinoma cells do not express caspase-3. *Breast Cancer Res. Treat.* (117), 219–221. <https://doi.org/10.1007/s10549-008-0217-9>.
- Junttila, M.R., Evan, G.I., 2009. p53-A Jack of all trades but master of none. *Nat. Rev. Cancer* 9 (11), 821–829. <https://doi.org/10.1038/nrc2728>.
- Karimian, A., Ahmadi, Y., Yousefi, B., 2016. Multiple functions of p21 in cell cycle, apoptosis and transcriptional regulation after DNA damage. *DNA Repair* 42, 63–71. <https://doi.org/10.1016/j.dnarep.2016.04.008>.
- Keller, S., Ong, Y.C., Lin, Y., Cariou, K., Gasser, G., 2020. A tutorial for the assessment of the stability of organometallic complexes in biological media. *J. Organomet. Chem.* 906, 121059 <https://doi.org/10.1016/j.jorganchem.2019.121059>.
- Kozlyuk, N., Lopez, T., Roth, P., Acquaye, J.H., 2015. Synthesis and the characterization of Schiff-base copper complexes: reactivity with DNA, 4-NPP and BNPP. *Inorg. Chim. Acta.* 428, 176–184. <https://doi.org/10.1016/j.jica.2014.12.034>.
- Laussac, J.P., Sarkar, B., 1984. Characterization of the copper(II) and nickel(II) transport site of human serum albumin. Studies of copper(II) and nickel(II) binding to peptide 1–24 of human serum albumin by carbon-13 and proton NMR spectroscopy. *Biochem* 23, 2832–2838. <https://doi.org/10.1021/bi00307a046>.
- Lee, Z.Y., Leong, C.H., Lim, K.U., Wong, C.C., Pongtheerawan, P., Arikrishnan, S.A., Tan, K.L., Loh, J.S., Foo, J.B., 2021. Induction of apoptosis and autophagy by ternary copper complex towards breast cancer cells. *Anti Cancer Agents Med. Chem.* 22 (6), 1159–1170. <https://doi.org/10.2174/1871520621666210726132543>.
- Li, D.D., Yagüe, E., Wang, L.Y., Dai, L.L., Yang, Z.B., Zhi, S., Zhang, N., Zhao, X.M., Hu, Y. H., 2019. Novel copper complexes that inhibit the proteasome and trigger apoptosis in triple-negative breast cancer cells. *ACS Med. Chem. Lett.* 10 (9), 1328–1335. <https://doi.org/10.1021/acsmchemlett.9b00284>.
- Loboda, A., Damulewicz, M., Pyza, E., Jozkowicz, A., Dulak, J., 2016. Role of Nrf2/HO-1 system in development, oxidative stress response and diseases: an evolutionarily conserved mechanism. *Cell. Mol. Life Sci.* 73 (17), 3221–3247. <https://doi.org/10.1007/s00018-016-2223-0>.
- Luu-Hoang, K.N., Anstee, J.E., Arnold, J.N., 2021. The diverse roles of heme oxygenase-1 in tumor progression. *Front. Immunol.* 12 (March), 1–14. <https://doi.org/10.3389/fimmu.2021.658315>.
- Marvalim, C., Datta, A., Lee, S.C., 2023. Role of p53 in breast cancer progression: an insight into p53 targeted therapy. *Theranostics* 13 (4), 1421–1442. <https://doi.org/10.7150/tno.81847>.
- Matson-Dzebo, M., Ariöz, C., Wittung-Stafshede, P., 2016. Extended functional repertoire for human copper chaperones. *Biomol. Concepts* 7, 29–39. <https://doi.org/10.1515/bmc-2015-0030>.
- McGivern, T.J.P., Afsharpour, S., Marmion, C.J., 2018. Copper complexes as artificial DNA metallo-nucleases: from Sigman's reagent to next generation anti-cancer agent. *Inorg. Chim. Acta.* 472, 12–39. <https://doi.org/10.1016/j.ica.2017.08.043>.
- Mosmann, T., 1983. Rapid colorimetric assay for cellular growth and survival: application to proliferation and cytotoxicity assays MTT-assay: cell viability. *J. Immunol. Methods* 65 (1–2), 55–63. [https://doi.org/10.1016/0022-1759\(83\)90303-4](https://doi.org/10.1016/0022-1759(83)90303-4).
- Muller, P.A.J., Vousden, K.H., 2013. p53 mutations in cancer. *Nat. Cell Biol.* 15, 2–8. <https://doi.org/10.1038/ncb2641>.
- Noh, S.J., Bae, J.S., Jamiyandorj, U., Park, H.S., Kwon, K.S., Jung, S.H., Youn, H.J., Lee, H., Jang, K.Y., 2013. Expression of nerve growth factor and heme oxygenase-1 predict poor survival of breast carcinoma patients. *BMC Cancer* 13, 516. <https://doi.org/10.1186/1471-2407-13-516>.
- Olsson, M., Zhivotovskiy, B., 2011. Caspases and cancer. *Cell Death Differ.* 18 (9), 1441–1449. <https://doi.org/10.1038/cdd.2011.30>.
- Podkalicka, P., Mucha, O., Jozkowicz, A., Dulak, J., Loboda, A., 2018. Heme oxygenase inhibition in cancers: possible tools and targets. *Contemp. Oncol.* 22 (1A), 23–32. <https://doi.org/10.5114/wo.2018.73879>.
- Sacchini, V., Norton, L., 2022. Escalating de-escalation in breast cancer treatment. *Breast Cancer Res. Treat.* 195 (2), 85–90. <https://doi.org/10.1007/s10549-022-06685-2>.
- Sarhangi, N., Hajjari, S., Heydari, S.F., Ganjizadeh, M., Rouhollah, F., Hasanazad, M., 2022. Breast cancer in the era of precision medicine. *Mol. Biol. Rep.* 49 (10), 10023–10037. <https://doi.org/10.1007/s11033-022-07571-2>.
- Sarpong-Kumankomah, S., Gailer, J., 2021. Application of a novel metallomics tool to probe the fate of metal-based anticancer drugs in blood plasma: potential, challenges and prospects. *Curr. Top. Med. Chem. (Sharjah, United Arab Emirates)* 21, 48–58. <https://doi.org/10.2174/156802662066620062802803540>.
- Shamloo, B., Usluer, S., 2019. p21 in cancer research. *Cancers* 11 (8), 1178. <https://doi.org/10.3390/cancers11081178>.
- Sung, H., Ferlay, J., Siegel, R.L., Laversanne, M., Soerjomataram, I., Jemal, A., Bray, F., 2021. Global cancer statistics 2020: GLOBOCAN estimates of incidence and mortality worldwide for 36 cancers in 185 countries. *CA A Cancer J. Clin.* 71, 209–249. <https://doi.org/10.3322/caac.21660>.
- Takahara, P.M., Rosenzweig, A.C., Frederick, C.A., Lippard, S.J., 1995. Crystal structure of double-stranded DNA containing the major adduct of the anticancer drug cisplatin. *Nature* 377, 649–652. <https://doi.org/10.1038/377649a0>.
- Tarin, M., Babaie, M., Eshghi, H., Matin, M.M., Saljooghi, A.Sh., 2023. Elesclomol, a copper-transporting therapeutic agent targeting mitochondria: from discovery to its novel applications. *J. Transl. Med.* 21, 745. <https://doi.org/10.1186/s12967-023-04533-5>.
- Theodossiou, T.A., Ali, M., Grigalavicius, M., Gallert, B., Dillard, P., Schink, K., Olsen, C., Wälchli, S., Inderberg, E., Kubin, A., Peng, Q., Berg, K., 2019. Simultaneous defeat of MCF7 and MDA-MB-231 resistances by a hypericin PDT-tamoxifen hybrid therapy. *Breast Cancer* 5 (13). <https://doi.org/10.1038/s41523-019-0108-8>.
- Van der Westhuizen, D., Bezuidenhout, D.I., Munro, O.Q., 2021. Cancer molecular biology and strategies for the design of cytotoxic gold(I) and gold(III) complexes: a tutorial review. *Dalton Trans.* 50, 17413–17437. <https://doi.org/10.1039/D1DT02783B>.
- Waks, A.G., Winer, E.P., 2019. Breast cancer treatment: a review. *JAMA* 321 (3), 288–300. <https://doi.org/10.1001/jama.2018.19323>.
- Wang, S., Konorev, E.A., Kotamraju, S., Joseph, J., Kalivendi, S., Kalyanaraman, B., 2004. Doxorubicin induces apoptosis in normal and tumor cells via distinctly different mechanisms. *J. Biol. Chem.* 279 (24), 25535–25543. <https://doi.org/10.1074/jbc.M400944200>.
- Yang, Y., Feng, Q., Luan, Ying, Liu, H., Jiao, Y., Hao, H., Yu, B., Luan, Yi, Ren, K., 2023. Exploring cuproptosis as a mechanism and potential intervention target in cardiovascular diseases. *Front. Pharmacol.* 14, 1229297 <https://doi.org/10.3389/fphar.2023.1229297>.
- Yue, X., Zhao, Y., Xu, Y., Zheng, M., Feng, Z., Hu, W., 2017. Mutant p53 in cancer: accumulation, gain-of-function, and therapy. *J. Mol. Biol.* 429, 1595–1606. <https://doi.org/10.1016/j.jmb.2017.03.030>.

- Zacharias, S.C., 2012. Structural, Physical and Biological Studies of Copper(II) and Rhenium(V) Schiff Base Complexes. University of KwaZulu-Natal, South Africa. Masters Thesis (MSc).
- Zehra, S., Tabassum, S., Arjmand, F., 2021a. Biochemical pathways of copper complexes: progress over the past 5 years. *Drug Discov. Today* 26 (4), 1086–1096. <https://doi.org/10.1016/j.drudis.2021.01.015>.
- Zehra, S., Cirilli, I., Silvestri, S., Gómez-Ruiz, S., Tabassum, S., Arjmand, F., 2021b. Structure elucidation, in vitro binding studies and ROS-dependent anti-cancer activity of Cu(II) and Zn(II) phthaloylglycinate(phen) complexes against MDA-MB-231 cells. *Metallomics* 13 (11), mfab064. <https://doi.org/10.1093/mtomcs/mfab064>.
- Zhang, W., Geiman, D.E., Shields, J.M., Dang, D.T., Mahatan, C.S., Kaestner, K.H., Biggs, J.R., Kraft, A.S., Yang, V.W., 2000. The gut-enriched Kruppel-like factor (Kruppel-like factor 4) mediates the transactivating effect of p53 on the p21(WAF1)/(Cip)1 promoter. *J. Biol. Chem.* 275 (24), 18391–18398. <https://doi.org/10.1074/jbc.C000062200>.